Стохастическое моделирование в прикладной математике и вычислительной физике.

К. К. Сабельфельд

Математический Центр в Академгороде, Новосибирский Государственный университет, Институт Вычислительной Математики и Математической Геофизики СО РАН

Математический центр в Академгородке
Семинар "Актуальные проблемы прикладной математики".
Новосибирск, 22.05.2020

- Introducton: Probabilistic approach, Randomization and simple examples.
- Large dimensions, and random projections. Johnson-Lindenstrauss lemma. Row action methods and acceleration by J-L lemma.
- An inverse retrieving problem, application to X-ray analysis of nanolayers.
- Probabilistic representations for PDEs. Random Walk on Spheres method. PDEs with random boundary conditions.
- Drift-diffusion-recombination systems for exciton transport in semiconductors. The Cathodoluminescence iimaging of dislocations.
- Diffusion and annihilation of electrons and holes: a system of nonlinear equations.
- Enzyme kinetics simulation
- Simulation of nanowire nucleation and growth by a molecular beam epitaxy method.

cations and apply randomized projection methods [10] which extend the randomized Kaczmarz method first suggested in [16].

In the present paper we further develop this family of methods. The idea behind this new class of stochastic methods is a randomized vector representation of the matrix iterations, and in using stochastic and double stochastic matrices for efficient randomized calculation of matrix iterations. This can be applied, in particular, in a random gradient based search strategy. The calculations are extremely simple and economic: for instance, to calculate a matrix vector product we do not use multiplications at all provided the system of equations is properly pre-processed; second, the variance of the stochastic estimators are small, which means, higher accuracy is achieved compared to the conventional Monte Carlo algorithms. To prepare the original equation $A\mathbf{x} = \mathbf{b}$ to the desired form, we undertake a transformation $\hat{A} = D_1 A D_2$ where $\hat{A}$ is a doubly stochastic matrix, and D_1, D_2 are diagonal matrices. This can be done by different methods, we use the classical balancing Sinhorn method [13] (see also [14], [15]. Here it is assumed that the matrix A is nonnegative without loss of generality. The methods suggested can be applied also for calculation of principal eigenvector of large matrices, for constructing a randomized stochastic gradient search method and many others.

2 Random vector estimators for stochastic matrix iterations

Let $\mathbf{b} \in \mathbf{R}^n$ be a nonnegative stochastic vector, and let A be a nonnegative $m \times n$ stochastic matrix which means, $\sum_{j=1}^n b_j = 1$, and $\sum_{j=1}^n a_{i,j} = 1$ for $i = 1, 2 \dots m$. In what follows, we denote by $A_{\rightarrow k}$ the kth row, and by $A_{\uparrow r}$ the rth column of the matrix A. Thus in this paper under column stochastic matrix we understand a nonnegative matrix whose all columns are stochastic vectors. The main random estimators will be constructed by using column stochastic matrices. A doubly stochastic matrix is defined as a nonnegative matrix whose all columns and rows are stochastic vectors.

So let us start our considerations with a stochastic column vector $\mathbf{b}$ and stochastic matrix A. A random unbiased vector estimator for the product $A\mathbf{b}$ is defined by the column $\boldsymbol{\xi} = A_{\uparrow k}$ where k is a random index chosen from $\{1, 2, \dots, n\}$ according to the probability distribution $p_i = b_i$, $i = 1, 2, \dots, n$. This follows from the simple fact that for any matrix A and arbitrary vector $\mathbf{v}$, the product $A\mathbf{v}$ can be written in the following form: $A\mathbf{v} = \sum_{i=1}^n v_i A_{\uparrow i}$. For a stochastic matrix A and stochastic vector $\mathbf{b}$ it implies that

$$A\mathbf{b} = \mathbf{E}\,\boldsymbol{\xi} = \mathbf{E}\{A_{\uparrow k}\,|p = \mathbf{b}\} \tag{2.1}$$

i.e., $\boldsymbol{\xi}$ is an unbiased estimator for $A\mathbf{b}$, indeed. Here $\mathbf{E}\{A_{\uparrow k}\,|p = \mathbf{b}\}$ means that the

expectation is taken over random columns chosen at random from the distribution $p = \mathbf{b}$.

Assume now, we have to calculate the second iteration, $A^2\mathbf{b}$. Then, from (2.1) we get

$$A^2\mathbf{b} = A\mathbf{E}\boldsymbol{\xi} = \mathbf{E}\mathbf{E}\{A_{\uparrow j} \,|\, p_2 = A_{\uparrow k}; p_1 = \mathbf{b}\} \,. \tag{2.2}$$

This representation says that first, we choose a random column $A_{\uparrow k}$ from the distribution $p_1 = \mathbf{b}$, and then choose a random column $A_{\uparrow j}$ from the distribution $p_2 = A_{\uparrow k}$, which is possible because the matrix A is stochastic. Thus an unbiased estimator of the second iteration $A\mathbf{b}$ is just a random column of the matrix chosen as described. Obviously, the unbiased estimator for the third iteration is obtained by the next random sampling of a random column $A_{\uparrow i}$ according the distribution $p_3 = A_{\uparrow j}$, etc. Generally, starting from the first iteration, say, $A\mathbf{x}$, we denote the unbiased estimator of $A\mathbf{x}$ by $\boldsymbol{\xi}_{j_1} = A_{\uparrow j_1}$ where the random index j_1 is sampled from $\mathbf{x}$; the estimator $\boldsymbol{\xi}_{j_2,j_1}$ for the second iteration $A^2\mathbf{x}$ is $\boldsymbol{\xi}_{j_2,j_1} = A_{\uparrow j_2}$ where the random index j_2 is sampled from the previously sampled column $A_{\uparrow j_1}$, etc., and for the kth iteration we write

$$\boldsymbol{\xi}_{j_k,j_{k-1},\ldots,j_2,j_1} = A_{\uparrow j_k} \tag{2.3}$$

where each next random column is sampled according to the previously sampled column. By the construction, we conclude that

$$\mathbf{E}\boldsymbol{\xi}_{j_k,j_{k-1},\ldots,j_2,j_1} = \mathbf{E}A_{\uparrow j_k} = A^k\mathbf{x}, \quad \text{for } k = 1, 2, \ldots \,. \tag{2.4}$$

Let us denote the ith component of a column-vector $A_{\uparrow j}$ by $(A_{\uparrow j})_i$.

Theorem 1. *For a stochastic initial vector* $\mathbf{x}$ *and stochastic matrix* A *the random estimator* $A_{\uparrow j_k}$ *for the iteration* $A^k\mathbf{x}$ *has the following uniform upper bound of the variance:*

$$D(A_{\uparrow j_k})_i \le \frac{1}{4}||A_{\to i}||^2 \quad i = 1, \ldots, n, \quad k = 1, \ldots, \,. \tag{2.5}$$

This can be easily verified by direct evaluation, using the fact that $q(1-q)$ for any $0 \le q \le 1$ reaches its maximum value of 1/4 at $q = 1/2$.

Corollary. *For doubly stochastic matrices,* $D(A_{\uparrow j_k})_i \le 1/4$ *is true for iterations of arbitrary order.*

Note that for any stochastic vector $\mathbf{v}$ and any square $n \times n$ stochastic matrix A, the random estimator for $A^T\mathbf{v}$ has the form $(A_{\to k})^T$ where the index k is

convergence. More details about different versions of this method can be found in [6], [7], [13], [15], [16].

The Markov chain-based methods use a minimum of computer memory, but, in addition to the strong restriction $\rho(|H|) < 1$, a clear disadvantage is the weak convergence rate of these methods. It should be noted that the restriction $\rho(|H|) < 1$ can be weakened, see [15], however the variance analysis of the Markov chain-based methods then becomes quite complicated.

In [17] we used a different type of stochastic algorithms which are based on unbiased estimators for iterations of the matrix $A = I - H$: $A\,b = E\,S\,b$ where S is an unbiased sparse random estimator of A. In these methods, each iteration involves a matrix vector multiplication, but the dimension of the iteration matrix is considerably smaller than that of the original matrix A. Generally, the idea to use a randomization of large matrices by a set of small random matrices is not new. It is successfully used for the low rank approximation [1], [8], [11], [14], [24] for the randomized iterative version of the Lanczos method [5], for matrix multiplication [3], [4], and for accelerating the method of the conjugate gradient method by randomizing the choice of the projection subspaces [18, 22]. In all these studies it was confirmed that the randomization is an extremely efficient tool when dealing with very large systems both with nonsingular quadratic and general singular rectangular matrices.

In our paper we suggest randomized versions of the projection method, in particular, a randomized block projection method, and a randomized version of the orthogonal projection method combined with the Johnson–Lindenstrauss dimension reduction.

The Johnson–Lindenstrauss theorem [9] asserts that any set of n points in d-dimensional Euclidean space can be embedded into k-dimensional Euclidean space where k is logarithmic in n and independent of d so that all pairwise distances are maintained within an arbitrarily small factor. The linear transformation can be done by a random matrix whose entries are independent standard Gaussian random variables. This transformation was essentially simplified in [1] by showing that this matrix can be changed with a matrix whose entries r_{ij} are independent discrete random variables with the distribution $P(\pm 1) = 1/6$, $P(0) = 2/3$ which greatly sparsifies the matrix. More precisely, Achlioptas' theorem is formulated as follows [1].

Theorem. *Suppose that A is an $n \times d$ matrix of n points in $\mathbb{R}^d$. Fix constants $\varepsilon, \beta > 0$, and choose an integer k such that*

$$k \geq \frac{4 + 2\beta}{\varepsilon^2 - \varepsilon^3/3} \log n.$$

Suppose that R is a random $d \times k$ matrix with entries r_{ij} belonging to the distribution

$$r_{ij} = \sqrt{3} \begin{cases} +1 & p = 1/6 \\ 0 & p = 2/3 \\ -1 & p = 1/6. \end{cases}$$

Define an $n \times k$ matrix $G = \frac{1}{\sqrt{k}} AR$, which is considered as a projection of A onto a k-dimensional subspace. For any row $\mathbf{u}$ in A, let $f(\mathbf{u})$ be the corresponding row in G. Then, for any distinct rows $\mathbf{u}, \mathbf{v}$ of A, we have

$$(1 - \varepsilon)\|\mathbf{u} - \mathbf{v}\|^2 \leq \|f(\mathbf{u}) - f(\mathbf{v})\|^2 \leq (1 + \varepsilon)\|\mathbf{u} - \mathbf{v}\|^2$$

with probability at least $1 - n^{-\beta}$.

In [2], the authors suggested a low-distortion embedding of L_2^d into $L_p^{O(\log n)}$ ($p = 1, 2$), called the Fast-Johnson–Lindenstrauss Transform (FJLT). The FJLT is faster than standard random projections and just as easy to implement. It is based upon the preconditioning of a sparse projection matrix with a randomized Fourier transform.

2 Randomized projection algorithms

2.1 Row action iteration process

The row action iteration process suggested first by Kaczmarz [10] can be proved to converge for any system of linear equations with nonzero rows, even when it is singular and inconsistent, and the arithmetic operations required in an iteration of the method are comparatively few (e.g., see [20]).

Let us consider a system of linear algebraic equations

$$Ax = b \tag{2.1}$$

where A is a rectangular $m \times n$ matrix with $m \geq n$, and $b \in \mathbb{R}^m$, $x \in \mathbb{R}^n$.

We further denote by a_i the i-th row of A, with the Euclidean norm $\|a_i\|$, and a_i^T is the relevant column-vector, the transpose of a_i, and assume that $\|a_i\| > 0$ for all i.

Our stochastic iterative process is written as follows

$$x_{k+1} = x_k + \omega_k \, E \, \frac{b_{\nu(i)} - (a_{\nu(i)} \cdot x_k)}{\|a_{\nu(i)}\|^2} \, a_{\nu(i)}^T, \quad k = 1, 2, \ldots \tag{2.2}$$

where ω_k are some parameters (could be random), the expectation E is taken over the distribution of random indices $\nu(i)$ whose values are sampled at random among

random subsets of indices lying in $(1, 2, \ldots, m)$. The distribution can be chosen so that the method converges with expected exponential rate, not depending on the number of equations in the system. The solver does not even need to know the whole system, but only some random rows of the matrix, therefore, it is well suited for solving very large systems of linear algebraic equations. Moreover, this method can be used for solving systems of linear equations coupled with systems of linear inequalities. Remarkably, the structure of the algorithm remains practically the same, see [21].

So assume we solve a coupled system of linear equations and inequalities

$$a_i^T x \le b_i \quad i \in I_{\le}, \tag{2.3}$$

$$a_i^T x = b_i \quad i \in I_{=}. \tag{2.4}$$

Let

$$\gamma_k^{(i)} = \begin{cases} [(a_i \cdot x_k) - b_i]^+ & if\ i \in I_{\le} \\ (a_i \cdot x_k) - b_i & if\ i \in I_{=}, \end{cases}$$

and write the iteration process in the form:

$$x_{k+1} = x_k - \frac{\gamma_k^{(\nu(i))}}{\|a_{\nu(i)}\|^2} a_{\nu(i)}^T, \quad k = 1, 2, \ldots. \tag{2.5}$$

It can be shown (e.g., see [21]) that this process is convergent, and

$$E[d^2(x_{k+1}, S)] \le \left(1 - \frac{1}{L^2 \|A\|_F^2}\right) d^2(x_k, S).$$

Here L is the Hoffmann constant defined by

$$d(x, S_b) \le L \| e(Ax - b)\|$$

where S_b is the set of possible solutions of our systems, $d(x, S_b)$ is the Euclidean distance from x to the set S_b, and $e(y)$ is defined as

$$e(y)_i = \begin{cases} y_i^+ & (i \in I_{\le}) \\ y_i & (i \in I_{=}). \end{cases}$$

2.2 Convergence analysis

The most important property of the iteration process (2.2) is that it converges for any system of linear equations with nonzero rows, even when it is singular and inconsistent (e.g., see the proof given in [20]). In [20] it is shown that in the inconsistent case, the process converges to the normal generalized solution x^* which minimizes the norm $\|Ax^* - b\|$.

2.3 Randomized version of the Kaczmarz method

In [19], the authors suggested to choose the rows in the Kaczmarz method at random, uniformly, or with some nonuniform distribution calculated proportional to the norms of the columns of the matrix A, i.e., the iteration process is arranged as follows

$$x_{k+1} = x_k + \frac{b_{\nu(i)} - (a_{\nu(i)} \cdot x_k)}{\|a_{\nu(i)}\|^2} a^T_{\nu(i)}, \quad k = 1, 2, \ldots \tag{2.13}$$

where $\nu(i)$ is the random index of the sampled row.

Clearly, the convergence may be slow, depending on the conditional number of the matrix A. So it is quite natural to undertake an intermediate averaging over a small number of hyperplanes, weighted with a relaxation parameter, i.e.,

$$x_{k+1} = x_k + \omega_k \, E \, \frac{b_{\nu(i)} - (a_{\nu(i)} \cdot x_k)}{\|a_{\nu(i)}\|^2} a^T_{\nu(i)}, \quad k = 1, 2, \ldots. \tag{2.14}$$

An important issue is the sampling of the random index $\nu(i)$. It can be sampled uniformly, or according to the norms of the rows, say, from the discrete probability density

$$p_k = \frac{\|a_k\|^2}{\sum_{k=1}^m \|a_k\|^2}, \quad k = 1, \ldots, m. \tag{2.15}$$

To sample from the density (2.15), we have suggested in [17] to use the Walker's method [23]. It takes only one call to the RAND generator, independent of the number of rows. It needs to prepare, out of the loop, two additional arrays of length m which takes about m arithmetic operations.

2.4 Randomized block projections algorithm

Assume we have chosen a partition of our matrix A into s row blocks, and the relevant partition of the vector b. So let us denote by A_i, $i = 1, \ldots, s$ the row blocks of the matrix A, $A = (A_1, \ldots, A_s)^T$, and b_i are here the relevant blocks of the vector b.

In the row projection method discussed above, the previous iteration was orthogonally projected successively on the hyperplanes. The projection of this vector on the intersection of hyperplanes defined by equations of the block A_i is defined by the projection operator

$$P_i = A_i^T (A_i A_i^T)^{-1} A_i.$$

It is assumed here that $(A_i A_i^T)^{-1}$ exist for all i.

So the solution process will be simply the method of successive projections applied to calculating the intersection of the sets

$$H_i = \{x : A_i x = b_i\}.$$

The randomized iteration method is based on a random sampling of the block, say, having a random index $v(i)$. Then the iteration step is obtained by the following projection:

$$x_{k+1} = x_k + A_{v(i)}^T (A_{v(i)} A_{v(i)}^T)^{-1} (b_{v(i)} - A_{v(i)} x_k).$$

Of course, the method assumes that the matrix $A_{v(i)} A_{v(i)}^T$ can be efficiently inverted. For instance, in the case of two row block sampling when the blocks consist of two rows, this inversion is explicit, and the method is easily implemented. Our calculations show that even in this simplest case the method converges much faster than the single row sampling (see Section 5). Note that the strategy of random sampling of pairs of equations may be different: one may sample them uniformly, each pair being two successive rows, or the pairs may be formed by random rows sampled according to the weights proportional to norms of the blocks, or they may be randomly chosen without repetition, etc. This sampling strategy depends of course of the structure of the matrix. For instance, in the case of band matrices it is often useful to sample larger blocks which are inverted by efficient direct solvers.

3 Acceleration technique based on random J–L-projection

Assume the system of linear equations $Ax = b$ has a unique solution x, where A is an $n \times n$ matrix. The approach suggested below can be applied to overdetermined systems with rectangular $m \times n$ matrices where $m > n$, the x vector is then a generalized normal solution.

As discussed in the Introduction, the Johnson–Lindenstrauss theorem can be used to accelerate the calculations in the original space $\mathbb{R}^n$ for very large n by random projection to $\mathbb{R}^s$ where s is much smaller than m and behaves like $s \simeq \log(m)$. Here we suggest an acceleration of the row projection method by using the J–L theorem to find, among the randomly chosen rows, an optimal row in that we find a hyperplane with the maximal distance to the current iteration x_k so that the distance $\|x_{k+1} - x_k\|_2$ is maximal. This simply follows from $\|x - x_{k+1}\|_2^2 = \|x - x_k\|_2^2 - \|x_k - x_{k+1}\|_2^2$. To calculate these distances in the original high dimension n may be costly, so the idea is simple: use the J–L projection, and calculate these distances in the new dimension s. By the Johnson–Lindenstrauss theorem, these distances are close to the relevant distances in the original dimension, with high probability. So when comparing the distances from the current point x_k to two

different hyperplanes in the original space $\mathbb{R}^n$ we know that the difference between these two distances is with high probability close to the difference between the relevant two distances in the new J–L transformed vector space $\mathbb{R}^s$. This implies, the problem of finding the hyperplane j which has a maximal distance from x_k among all the hyperplanes, can be replaced with the same problem in the J–L transformed space.

The formal considerations start by rewriting $Ax = b$ as $ARR^T x = b$ where R is an $n \times s$ orthogonal matrix. Then, in the spirit of the J–L theorem, we substitute the matrix R with a random matrix whose entries are independent random variables having zero mean and variance $\frac{1}{s}$. Then, in the space of vectors $y = R^T x$, we construct our random row projection algorithm.

This leads us to the following version of the randomized row projection method.

New version based on the Johnson–Lindenstrauss projection theorem

1. Take an $m \times n$ matrix A, and a column vector b, choose an integer parameter $s = 8\log(m)/\varepsilon^2$, ε is the desired accuracy, which corresponds to the probability level $1 - m^{-2}$ in the J–L theorem, and the initial approximation x_0.

2. We aim at an approximation of the solution x to $Ax = b$.

3. Set $k = 0$, generate an $n \times s$ random matrix R satisfying the independence and symmetry condition (as described in the Introduction), say, the Achlioptas' sparse matrix R mentioned in the Introduction, or a Gaussian matrix $R = \{g_{ij}\}$ where the entries g_{ij} are independent zero mean Gaussian random numbers with variance $\frac{1}{s}$, and calculate the rows $h_i = (AR)_i = a_i R$.

4. Sample a set of $N = m$ rows at random, say, according to $p_i = \|a_i\|_2^2/\|A\|_F^2$, (by the Walker's method which needs only one call of the RANDOM generator). Uniform sampling is also possible. Note that N can be taken less than m which implies that the random search of rows is carried out only among a part of all the rows.

For each row, calculate the distance $\Delta_i = |b_i - (h_i, R^T x_k)|/\|h_i\|_2$ and choose a_j as the row with the maximal Δ_j. This row is used to calculate the next projection step in our iteration process (3.1).

A hedging step can be introduced here to prevent the case that the chosen j is worse than the random row actually used in the calculation of the projection. So along with the chosen a_j take also an arbitrary row a_p in the set of chosen rows, and calculate

$$\bar{\Delta}_j = \frac{|b_j - (a_j, x_k)|}{\|a_j\|_2}, \quad \bar{\Delta}_p = \frac{|b_p - (a_p, x_k)|}{\|a_p\|_2}.$$

If $\bar{\Delta}_p > \bar{\Delta}_j$, set $j = p$.

Calculate the projection:

$$x_{k+1} = x_k + \frac{b_j - (a_j, x_k)}{\|a_j\|_2^2} a_j^T. \tag{3.1}$$

5. $k = k + 1$, goto 4.

According to the Johnson–Lindenstrauss theorem, if we take $s = 8\log(m)/\varepsilon^2$, then for two different rows i and j we get

$$(1-\varepsilon)\|a_i - a_j\|^2 \le \|a_i R - a_j R\|^2 \le (1+\varepsilon)\|a_i - a_j\|^2$$

with high probability of about $1 - m^{-2}$.

Notice that using these estimations, one easily estimates the errors in the calculation of the true distances $\bar{\Delta}_i$: $|\bar{\Delta}_i - \Delta_i| = O(\varepsilon)$, but we need also estimations of the relevant variances.

All we need in the algorithm is the comparison of the distances from the current point $R^T x_k$ to two different hyperplanes described by the relevant two different rows of the matrix AR. But of main importance is the variance of the calculated random distances, and even more, how the random distances are concentrated around the true values. The Johnson–Lindenstrauss theorem gives such concentration results only for two arbitrary rows h_i and h_j in the transformed matrix AR. But it says nothing about the scalar products $(h_i, R^T x_k)$ and $(h_j, R^T x_k)$ that define the distances. In our algorithm, we care about the difference between $\bar{\Delta}_i$ and Δ_i for each $i = 1, \dots, N$ that are defined by the scalar products (a_i, x_k) and $(h_i, R^T x_k)$, respectively. So let us study this difference.

Let us introduce the notation for the following quantities:

$$m_i^2 = \|a_i\|^2 = \sum_{j=1}^{n} a_{i,j}^2, c_{ij} = (a_i \cdot a_j) = a_i a_j^T,$$
$$d_{ij}^2 = \|a_i - a_j\|^2 = m_i^2 + m_j^2 - 2c_{ij}.$$

By direct calculations (e.g., see [12]) and [22] one gets for the transformed vectors $h_i = a_i R$ the following relations:

$$E\|h_i\|^2 = \|a_i\|^2 = m_i^2, \qquad \mathrm{Var}\|h_i\|^2 = \frac{2}{s} m_i^4,$$
$$E\|h_i - h_j\|^2 = d_{ij}^2, \qquad \mathrm{Var}\|h_i - h_j\|^2 = \frac{2}{s} d_{ij}^4,$$
$$E(h_i \cdot h_j) = (a_i \cdot a_j) = c_{ij}, \qquad \mathrm{Var}(h_i \cdot h_j) = \frac{1}{s}(m_i^2 m_j^2 + c_{ij}^2).$$

The x-ray diffraction analysis of the depth profile of thin films is based on the equation

$$\left| \int_a^b \exp\{iqz\} p(z) dz \right|^2 = f(q)$$

where q is the view angle, and dz is the height element of the epitaxial film.
Let us turn to a discrete approximation of this equation. We choose a subdivision of the interval $[a, b]$: $\{z_j, j = 1, \ldots, n\}, z_1 = a, z_n = b$.

Then,

$$\left|\int_a^b \exp\{iqz\}p(z)dz\right|^2 \simeq \left|\sum_{j=1}^{n}\left(\cos(qz_j)+i\sin(qz_j)\right)p(z_j)\delta z_j\right|^2 =$$

$$= \left|\sum_{j=1}^{n}\cos(qz_j)p(z_j)\delta z_j + i\sum_{j=1}^{n}\sin(qz_j)p(z_j)\delta z_j\right|^2 =$$

$$\left(\sum_{j=1}^{n}\cos(qz_j)p(z_j)\delta z_j\right)^2 + \left(\sum_{j=1}^{n}\sin(qz_j)p(z_j)\delta z_j\right)^2 =$$

$$\sum_{j=1}^{n}\left(p(z_j)\right)^2\delta z_j^2 + 2\sum_{j=1}^{n}\sum_{k=j+1}^{n}\cos(q(z_j-z_k))p(z_j)\delta z_j p(z_k)\delta z_k \quad (10)$$

Let $x_i = p(z_i)\delta z_i$, then

$$\sum_{j=1}^{n} x_j^2 + 2\sum_{j=1}^{n}\sum_{k=j+1}^{n} \cos(q(z_j - z_k))x_j x_k \simeq f(q). \qquad (11)$$

Now let us choose a subdivision of the parameter q: $\{q_i, i = 1, \ldots, m\}$ on a segment (c, d) where the function $f(q)$ is defined. This leads to the following system of equations

$$\sum_{j=1}^{n} x_j^2 + 2\sum_{j=1}^{n}\sum_{k=j+1}^{n} \cos(q_i(z_j - z_k))x_j x_k = f(q_i),\ i = 1, \ldots, m. \qquad (12)$$

Additional constrains to be satisfied by the solutions of (12) read

- the solution $\{z_j, j = 1, \ldots, n\}$ is a step function,
- the number of steps on (a, b) is prescribed, as well as the points of jumps are known.

The system of equations which has been solved can be written as

$$F_i(x) = y^{\delta,i},\ i = 0, \ldots, N-1,$$

where $y^{\delta,i}$ are the measurements including noise, satisfying

$$\|y^{\delta,i} - y^i\| \leq \delta^i, i = 0, \ldots, N-1.$$

The system of projection equations has the form:

$$x_{n+1} = x_n - F'_{[n]}(x_n) * \left(F_{[n]}(x_n) - y^{\delta,[n]}\right) .$$

where F' is the Jacoby matrix.

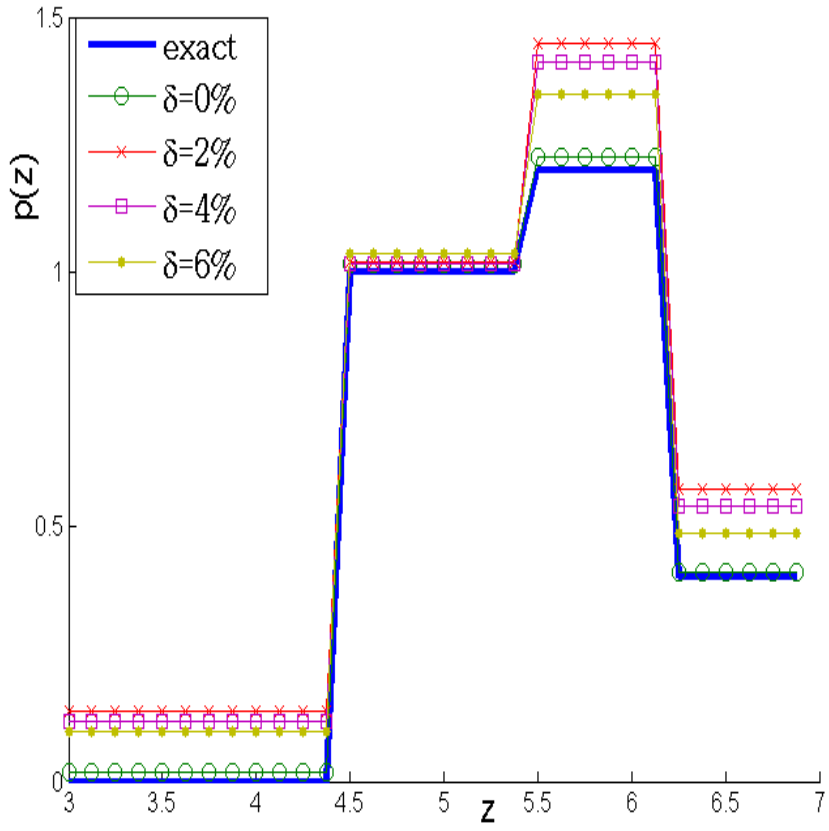

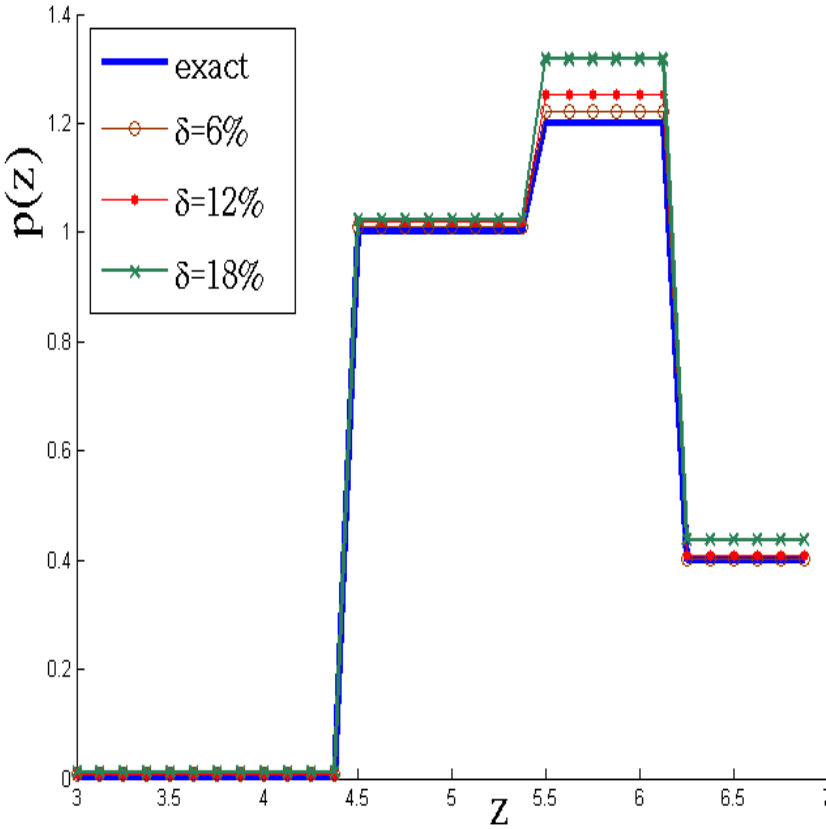

Рис.: Height profiles of the thin film: calculations have been carried out for $m = 128, n = 32$ by the genetic algorithm (left panel) and projection method (right panel).

Another type of stochastic projection technique: the equation

$$\left| \int_a^b \exp(iqz) p(z) dz \right|^2 = f(q)$$

is again, as above, written in an approximated discrete form. Introducing the grid $\{z_j, j = 1, \ldots, n\}, z_1 = a, z_n = b$ и $\{q_i, i = 1 \ldots, m\}, q_1 = c, q_m = d$ we turn to the system of equations

$$\left| \sum_{j=1}^{n} \cos(q_i z_j) p(z_j) \delta z_j + i \sum_{j=1}^{n} \sin(q_i z_j) p(z_j) \delta z_j \right|^2 = f(q_i), \quad i = 1 \ldots, m$$

which in a matrix form reads

$$y = \|Ax\|^2,$$

where $y \in \mathbb{C}^m, x \in \mathbb{C}^n$ и $A \in \mathbb{C}^{m \times n}$,

$$y_i = f(q_i), x_j = p(z_j), a_{i,j} = \cos(q_i z_j) \delta z_j + i \sin(q_i z_j) \delta z_j \ .$$

The iterations are constructed as follows.

Choose an initial vector x_0.
For $l = 0, \ldots$ do

1. Choose a row a_r of the matrix A, where the index r is sampled at random from some distribution, e.g., simply from a uniform distribution. (Another form of the distribution will be considered below).
2. Calculate the angle $\theta_l = \angle(a_r, x_l)$
3. calculate the next iteration $x_{l+1} = x_l + \frac{\sqrt{y_r} \exp i\theta_l - (a_r, x_l)}{\|a_r\|_2^2} a_r^*$.
   In each iteration, additional restrictions are incorporated:
4. $x_{l+1}^i \geq 0$, if all components are non-negative.
5. Stopping the iterations.

The accuracy is controlled by

$$\epsilon_l = \frac{\sqrt{\sum_{k=1}^{m}(\log(y_k) - \log(a_k x_l))^2}}{\sqrt{\sum_{k=1}^{m}(\log(y_k))^2}}.$$

If $\epsilon_{l+1} \geq \epsilon_l$, then $x_{l+1} = x_l$ with some prescribed probability. The uniform sampling of the random rows is simple but it is not the best choice. More efficient random choice in our calculations was constructed as follows. We introduce the random distribution by

$$p_k = \frac{[\log(y_k) - \log(a_k x_l)]^2}{\sum_{k=1}^{m}[\log(y_k) - \log(a_k x_l)]^2}\ , \quad k = 1, 2, \ldots, m\ .$$

Sampling the row from this distribution is carried our by the Walker's sampling method which has been implemented to get a row sampled using only one call of the rand() generator.

In our test example, $h(z)$ is assumed to be a nonnegative piecewise constant function, the positions of jumps are given, the problem is to recover the heights of the step function h. We have taken a test piecewise constant function as shown in Figure 2, left panel. The quadratic operator transforms this function to a signal, the right-hand side of the equation, shown in the right panel of the figure 2. Then, this signal was recovered by the algorithm presented, and the obtained solution was superimposed on the exact step function in the left panel. It is seen that the accuracy is extremely high although the size of the approximating system was $n = 192$ by $m = 10240$. Indeed, it is seen that the exact and calculated curves are practically coincident.

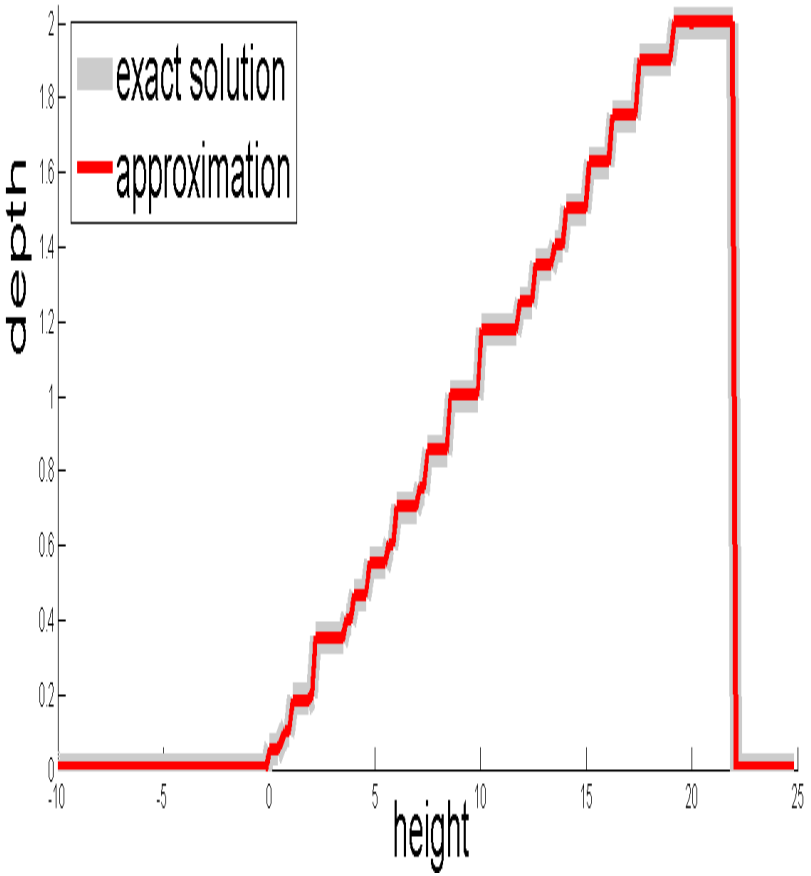

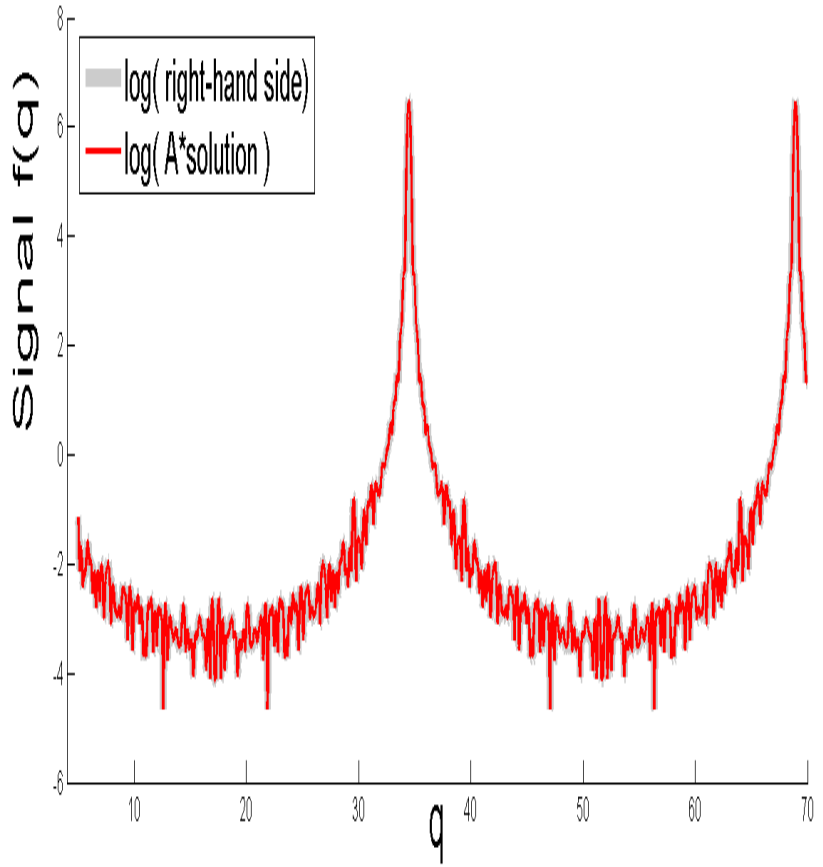

Рис.: Calculations made for $m = 10240, n = 192$, the number of steps 26. The exact solution, the step function, is superimposed with the solution obtained by the algorithm described (left panel).

8.3 The Random Walk on Spheres algorithm

8.3.1 The Random Walk on Spheres process for the Dirichlet problem

We show now that the spherical mean value relation and the Monte Carlo procedure of calculating the iterations of the spherical mean operator described above can be used to give a numerical method for solving the Dirichlet problem for the Laplace equation:

$$\Delta u(x) = 0, \quad x \in G, \qquad u|_\Gamma = \varphi \ .$$

We recall the definitions given in Chapter 2: $d(x)$ is the distance from the point x to the boundary of the domain, and Γ_ε is defined as the set

$$\Gamma_\varepsilon = \{x \in G : \ d(x) < \varepsilon\}.$$

Let us define the Random Walk on Spheres process in the domain G. It starts at the point x, and the states $y_1, y_2, \ldots$ are constructed as in the Markov chain $Y_k(x)$ described above, where $r_i = d(y_{i-1})$, and the process stops if after, say, N_ε steps, $y_{N_\varepsilon} \in \Gamma_\varepsilon$. We denote the Random Walk on Spheres process by Y_ε. This process is also called the ε-spherical process. It can be defined as a sequence of random points

$$y_i = y_{i-1} + d(y_{i-1})\omega_i, \ i = 1, 2, \ldots, \ y_0 = x,$$

where $\{\omega_i\}$ is a sequence of independent unit isotropic vectors. The last random state is y_{N_ε} such that $y_{N_\varepsilon} \in \Gamma_\varepsilon$ (see Fig. 8.1).

The main properties of the Random Walk on Spheres process Y_ε are well known (see, for example, [160]). The following property is important since it shows that the process rapidly converges to the boundary: for bounded domains of arbitrary dimension and practically arbitrary boundaries (for details, see [160]) the random process Y_ε with probability one converges to the boundary even if $\varepsilon = 0$ while the mean number of steps to reach Γ_ε is $O(\ln(\varepsilon))$ as $\varepsilon \to 0$. For unbounded domains, see [169].

Using the converse spherical mean value theorem (see Theorem 2.5) and the random estimators for the iterations I_k, it is possible to construct the random estimator for the Dirichlet problem. Indeed, since the Random Walk on Spheres process reaches the set Γ_ε with probability one in a finite number of steps, it follows from the converse spherical mean value theorem (see Section 2.1.2) that

$$u(x) = \mathbb{E}u(y_{N_\varepsilon}) \ .$$

Choosing ε small enough, in practice one uses

$$u(x) \approx \mathbb{E}\varphi(\bar{y}_{N_\varepsilon})$$

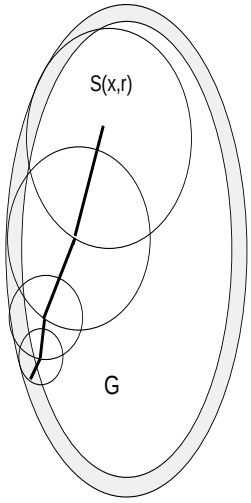

Figure 8.1. The random ε-spherical process starting at x, the center of the first sphere $S(x,r)$. In this illustration we see one trajectory which, after 4 steps, comes to Γ_ε.

where $\bar{y}_{N_\varepsilon}$ is the point of the boundary closest to the last state $y_{N_\varepsilon} \in \Gamma_\varepsilon$.

The convergence of the Random Walk on Spheres method follows from the estimation of the relevant integral operator generated by the spherical mean value relation. We present here the proof for the case of bounded domain $G \subset \mathbb{R}^3$ and domains with $d^* < \infty$, where d^* is a sphere of maximal radius which can be inscribed into the domain G.

More formally,

$$d^* = \sup_{x \in G} d(x),$$

where $d(x)$ is the radius of the sphere $S(x, d(x))$ centered at the point x inscribed into G; obviously, $d(x)$ equals the distance from the point $x \in G$ to Γ, the boundary of G. Let $P_\varepsilon(x)$ be the probability that the random point uniformly distributed on a sphere $S(x,r) \subset G$ hits the set Γ_ε. Simple arguments lead to the uniform estimation [50]

$$P_\varepsilon(x) \leq \frac{\varepsilon^2}{4(d^*)^2} \ .$$

Using this estimation we get the convergence for the domains with $d^* < \infty$. To this end we first write down a formal integral equation generated by the spherical mean value relation (e.g., see [50]).

Theorem 5. *Let $u(\mathbf{x}, y)$, $\mathbf{x} = (x_1, \ldots, x_{n-1})$ be a random field defined in the half-space $D_+ = \mathbb{R}^n_+$ as a harmonic function with the boundary condition $u|_{y=0} = g$ where g is a zero mean homogeneous random field on the boundary $\{y = 0\}$ with the correlation function $B_g(\mathbf{x})$ which is bounded in dimension $n = 2$, or tends to zero as $|\mathbf{x}| \to \infty$ if $n > 2$. Then $B_u(\mathbf{x}, y) = B_u(\mathbf{x}_2 - \mathbf{x}_1, y_1 + y_2)$, the correlation function of the solution, is a harmonic function in $\mathbb{R}^n_+$, and is related to B_g by the Poisson type formula:*

$$B_u(\mathbf{x}_2 - \mathbf{x}_1, y_1 + y_2) = \frac{\Gamma(n/2)}{\pi^{n/2}} \int\limits_{\partial D_+} \frac{(y_1 + y_2)\, B_g(\mathbf{x}')\, dS(\mathbf{x}')}{[(\mathbf{x}' - (\mathbf{x}_2 - \mathbf{x}_1))^2 + (y_1 + y_2)^2]^{n/2}} \,. \quad (2.37)$$

The proof is obtained by the same Fourier transform technique we used above.

Let us consider a transient drift-diffusion-recombination equation

$$\frac{\partial u(\mathbf{x},\tau)}{\partial \tau} = D\Delta u + \nabla\cdot(\mathbf{v}n) - \lambda^2 u + \delta(\tau)\delta(\mathbf{x}-\mathbf{x}_0), \quad \tau\in[0,t] \quad (1)$$

with zero initial conditions, $u(\mathbf{x},0)=0$, and relevant homogeneous boundary conditions. We consider here a general case, the Robin boundary conditions

$$(\mathbf{J}\cdot\boldsymbol{\nu}_k + S_k u\big|_{\Gamma_k} = 0, \qquad k=1,\dots m\ , \qquad (2)$$

where $\mathbf{J} = D\nabla u + \mathbf{v}\,u$, $\boldsymbol{\nu}_k$ are outward surface normal unit vectors, and S_k stand for the surface recombination velocities.
The total number of excitons annihilating at the relevant surfaces are obtained by integration of the fluxes over the time and surfaces, i.e.,

$$I_k(\mathbf{x}_0,t) = -\int_0^t d\tau \int_{\Gamma_k} \mathbf{J}\cdot\nu_k\, d\sigma_k\ , \qquad k=1,\dots m\ , \qquad (3)$$

Катодолюминесценция (CL & EBIC)

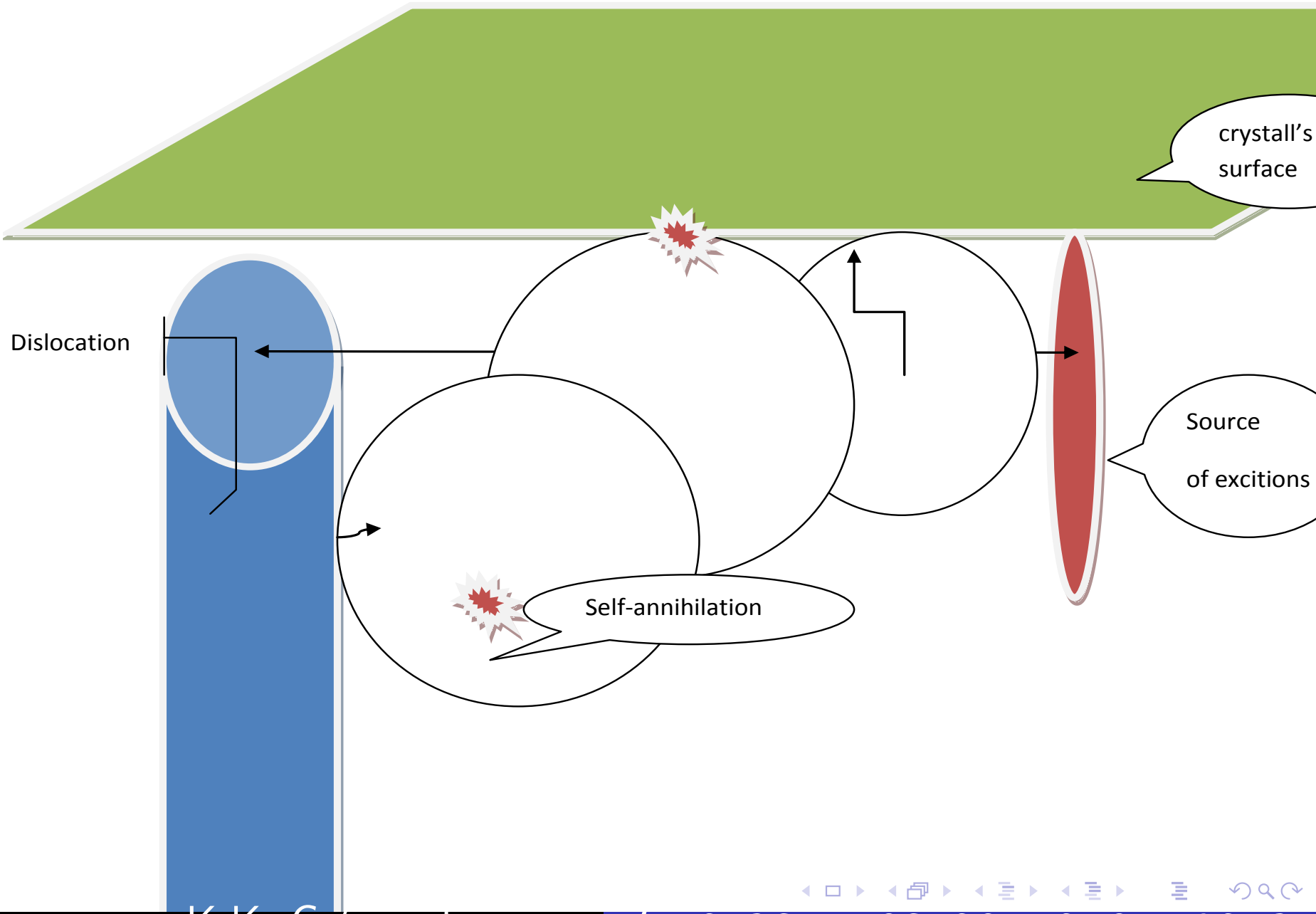

Катодолюминесценция (CL & EBIC)

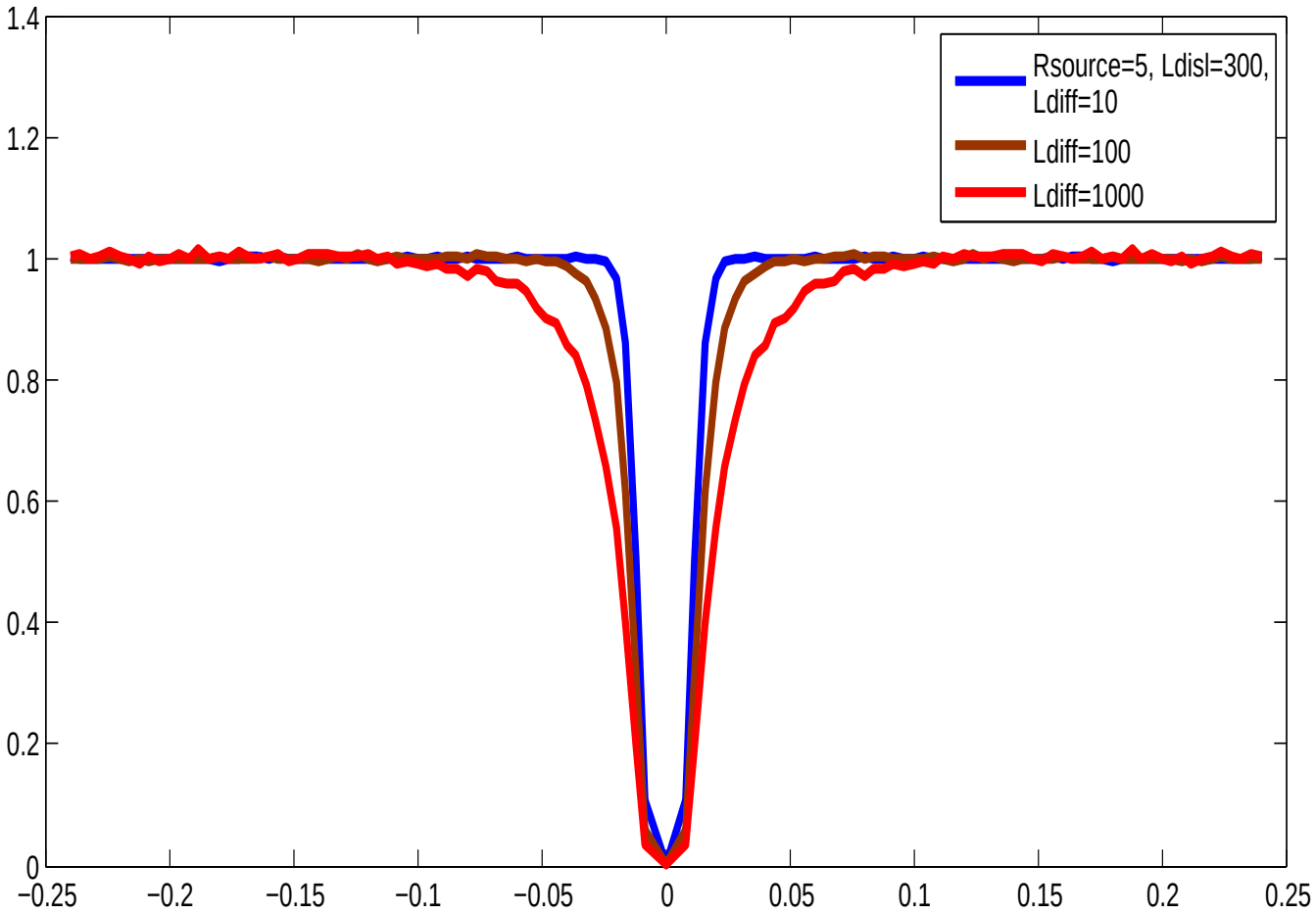

We consider a boundary value problem adjoint to the direct one, a homogeneous equation in a backward time $\tilde{\tau} = t - \tau$

$$\frac{\partial w}{\partial \tilde{\tau}} = D\Delta w - \mathbf{v} \cdot \nabla w - \lambda^2 w, \quad \tilde{\tau} \in [0, t] \quad (\tau \in [t, 0]) \tag{4}$$

with the initial condition $w(\mathbf{x}, 0) = 0$, and boundary conditions

$$(D\nabla w \cdot \boldsymbol{\nu}_k + S_k w)\big|_{\Gamma_k} = S_k \delta_{ik} \tag{5}$$

where δ_{ik} is the Kronecker symbol.
The fluxes $I_k(\mathbf{x}_0, t)$ are functions of the point $\mathbf{x}_0$, the position where the instantaneous point source is placed, and time t measured from the time instant $\tau = 0$ when the exciton was released. The next reciprocity theorem states that the flux $I_k(\mathbf{x}_0, t)$ coincides with $w(\mathbf{x}_0, t)$, the solution of the adjoint problem at the time $\tilde{\tau} = t$ which is the time where the initial conditions for the direct equation are posed.

The general reciprocity Theorem.

Assume we are given the direct (1), (2), and adjoint (3), (4) problems, as formulated above. Then

$$w(\mathbf{x}_0, t) = -\int_0^t d\tau \int_{\Gamma_k} \mathbf{J} \cdot \boldsymbol{\nu}_k \, d\sigma_k \tag{6}$$

where $\mathbf{J} = D\nabla u + \mathbf{v}u$.

Theorem. Spherical integral relation.

The solution $w(\mathbf{x}, t)$ of the adjoint drift-diffusion-reaction equation satisfies the spherical integral relation for any sphere $S(\mathbf{x}_0, R) \subset G$

$$w(\mathbf{x}_0, t) = Q_R \int_0^t \int_0^\pi \int_0^{2\pi} w(\mathbf{x}_0 + R\,\boldsymbol{\zeta}, t-\tau)\, p_\kappa(\theta, \varphi; \gamma, \beta)\; p_t(\tau)\, d\varphi\, d\theta\, d\tau\,, \tag{7}$$

where $Q_R = Q_1\, Q_2$,

$$Q_1 = \frac{\mu R/\sqrt{D}}{\sinh(\mu R/\sqrt{D})}\,, \quad \mu = \sqrt{\lambda^2 + |\mathbf{v}|^2/4D}\,, \tag{8}$$

$$Q_2 = \frac{\sinh(\kappa)}{\kappa}, \quad \kappa = |\mathbf{v}|R/2D\,, \tag{9}$$

and $p_t(\tau)$, the probability density of the first passage time, and $p_\kappa(\theta, \varphi; \gamma, \beta)$, the probability density of the exit point on the sphere are given by the following explicit expressions

$$p_t(\tau) = \frac{2}{Q_1} \sum_{n=1}^{\infty} (-1)^{n+1} \frac{\pi^2 n^2 D}{R^2} \exp\left\{ -\left(\frac{\pi^2 n^2 D}{R^2} + \frac{|\mathbf{v}|^2}{4D} + \lambda^2 \right) \tau \right\}, \tag{10}$$

$$p_\kappa(\theta, \varphi; \gamma, \beta) = \frac{1}{4\pi Q_2} \exp\left\{ \kappa [\sin\theta \sin\gamma \cos(\varphi - \beta) + \cos\theta \cos\gamma] \right\} \sin\theta \, . \tag{11}$$

In the coordinate system where the Z-axis coincides with the direction of the velocity,

$$p_\kappa(\theta, \varphi) = \frac{1}{4\pi Q_2} \sin\theta \, \exp\left\{ \kappa \cos\theta \right\}, \quad 0 \le \theta \le \pi, \; 0 \le \varphi \le 2\pi \, . \tag{12}$$

Péclet number $\kappa = \frac{|\mathbf{v}|R}{2D}$: $\kappa = 1$ (blue), 20 (green), and 80 (red).

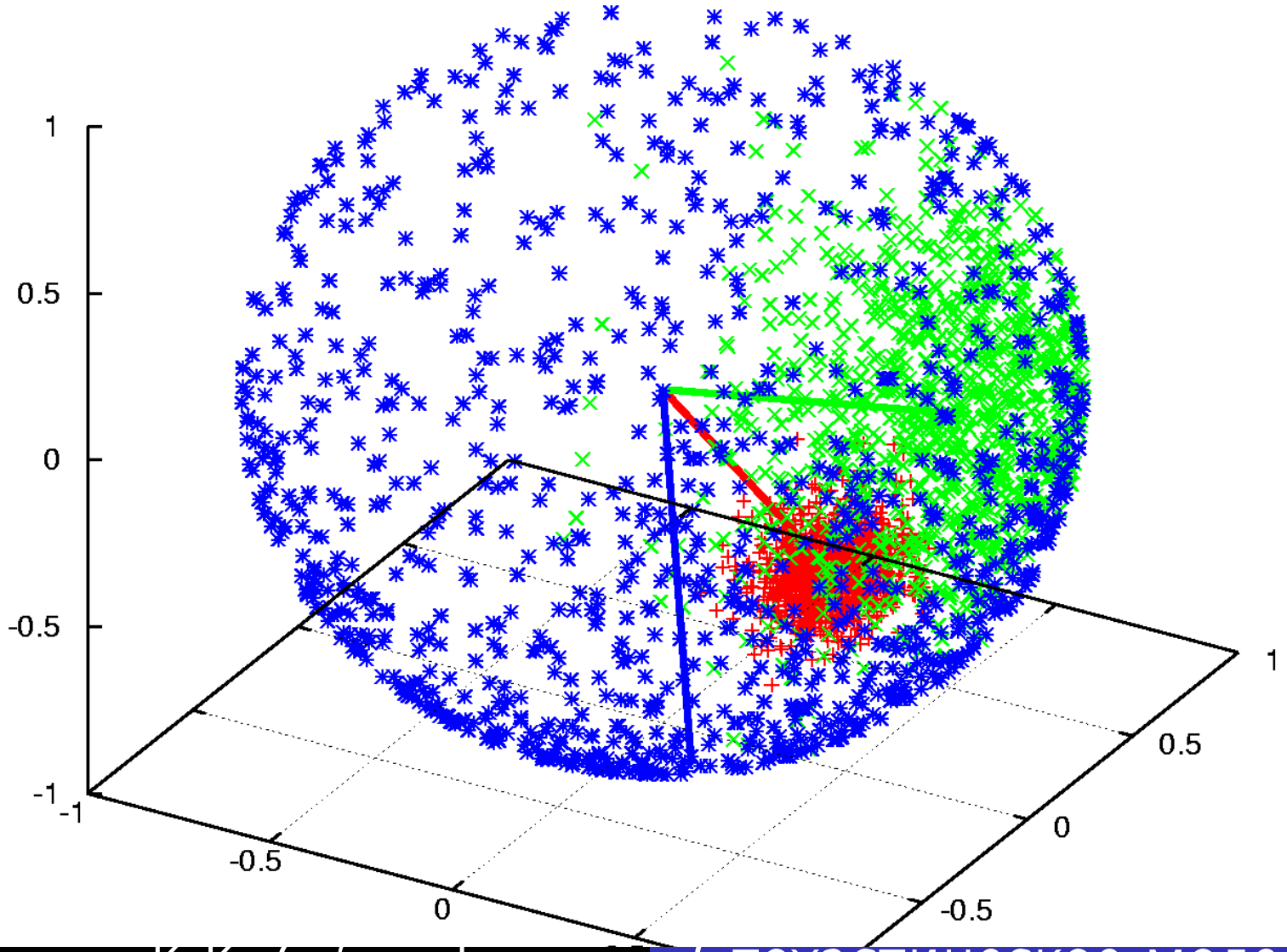

Drift velocity field around a threading dislocation

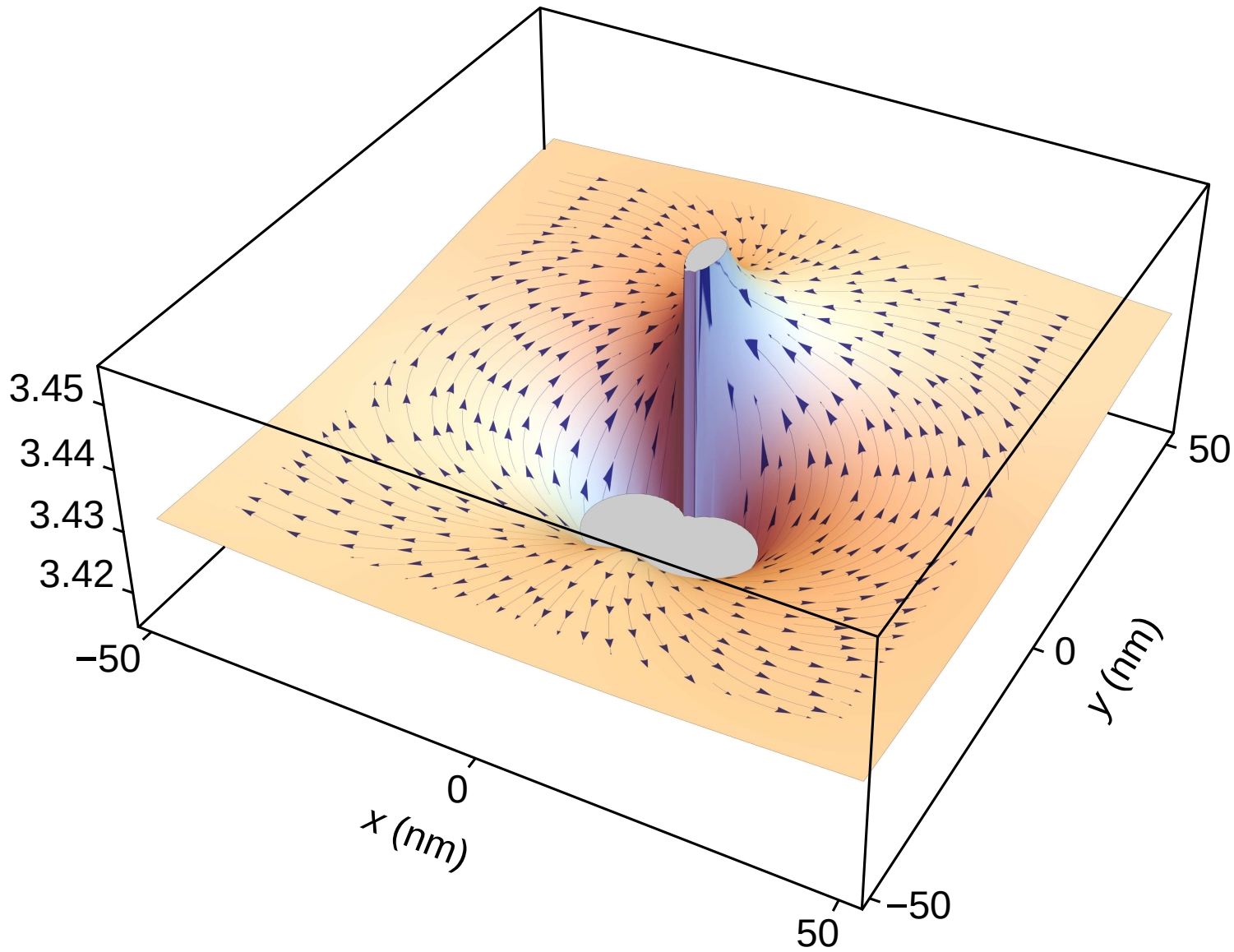

Cathodoluminescence maps and simulation results

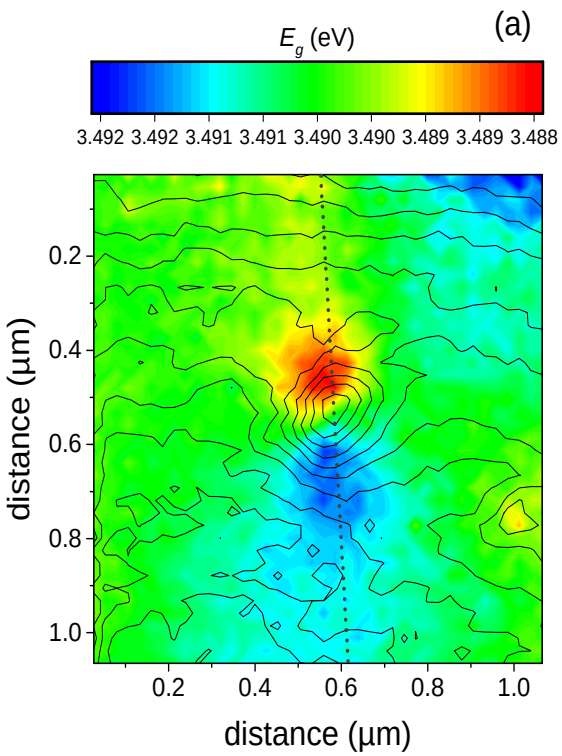

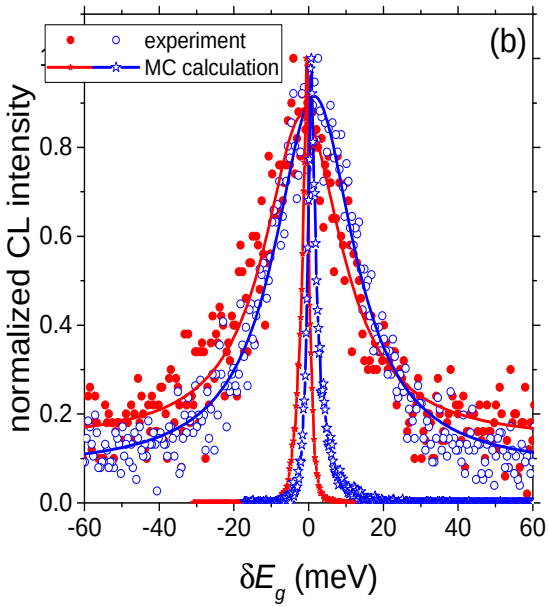

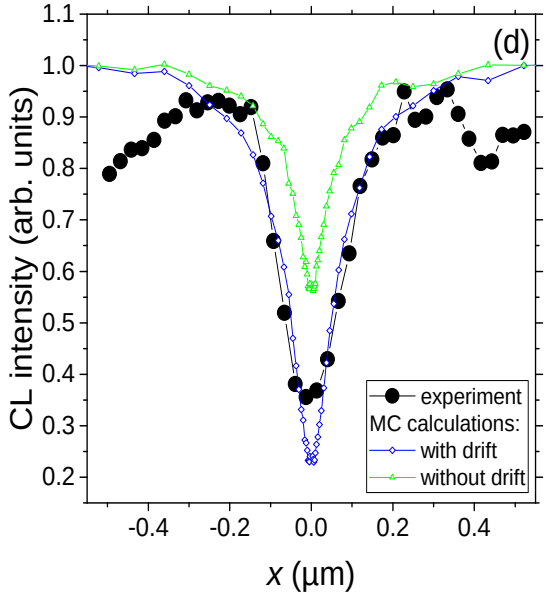

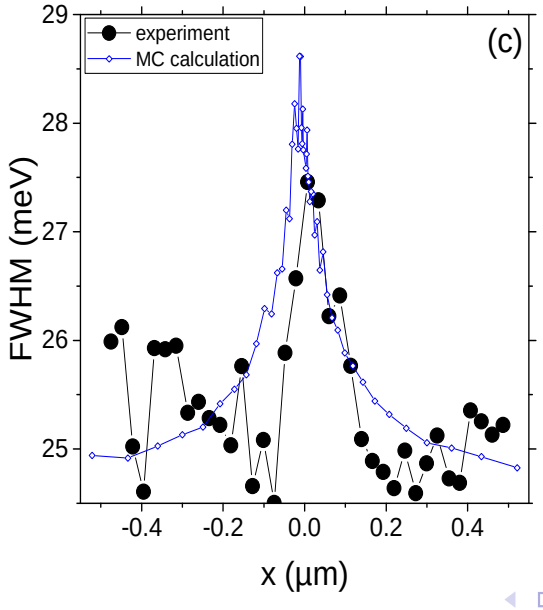

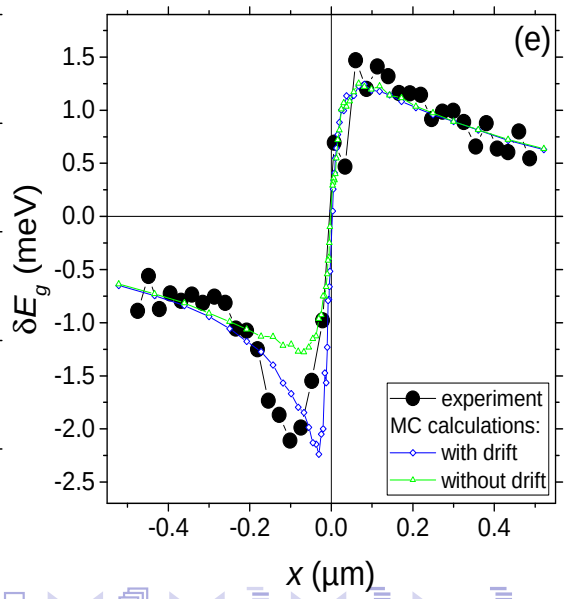

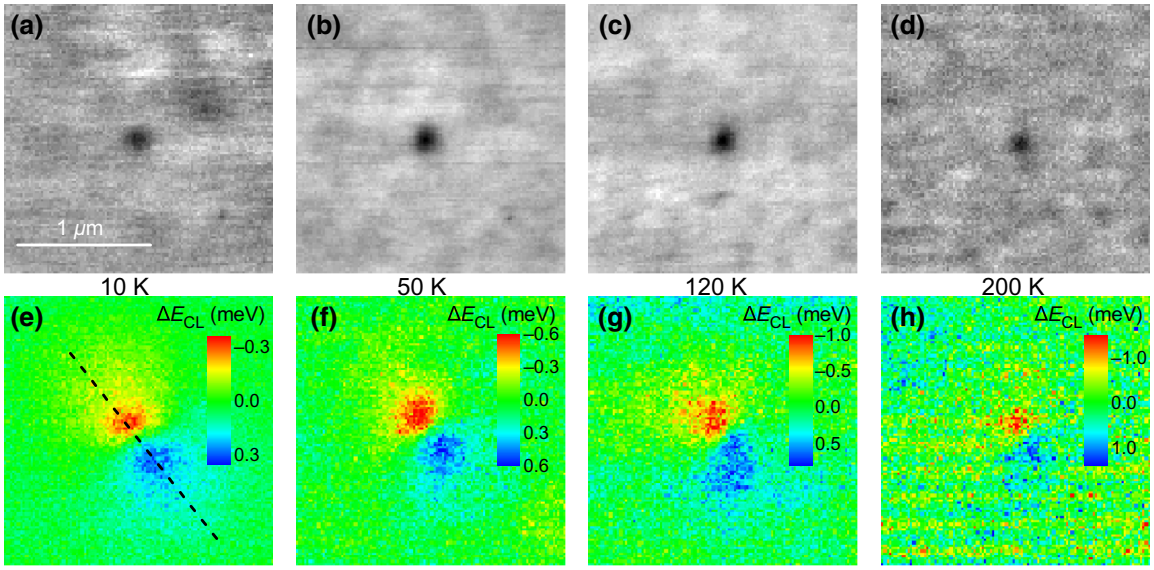

FIG. 3. Two-dimensional spatial maps of the (a)–(d) spectrally integrated CL intensity and (e)–(h) CL spectral-line positions for temperatures between 10 and 200 K around the selected threading dislocation. The dashed line in (e) indicates the direction of the line scans shown in Figs. 5(a) and 5(b). The scale bar in (a) applies to all maps.

from donor-bound exciton recombination [37] and the low-energy shoulder originating from acceptor-bound excitons, as well as from the two electron satellites of the donor-bound exciton [38], respectively, as shown in Fig. 2 (for maps acquired at 50, 120, and 200 K, no bound-exciton transition is observed and the fits to the free A-exciton line [39,40] are done with a single Lorentzian).

The sharp lines in Fig. 2 are resolution limited, with a full width at half maximum (FWHM) of 3 meV. The accuracy of the spectral positions of the lines is governed by statistical fluctuations of the CL intensity and amounts to 0.04 meV, as obtained from the fits shown in Fig. 2. The lines broaden with increasing temperature and reach a FWHM of 25 meV at 200 K. The accuracy then reduces to 0.4 meV, because of larger statistical fluctuations of the intensity. Since the line shifts in the vicinity of the dislocation also increase with temperature, as is demonstrated below, the accuracy is still sufficient to systematically study both the CL intensity and the line positions. However, the measurements at temperatures above 200 K are too noisy for a reliable analysis.

For each temperature, the fits yield maps of the spectrally integrated intensity of the dominant exciton transition and its spectral position, as shown in Figs. 3(a)–3(d) and Figs. 3(e)–3(h), respectively. The maps clearly reveal the reduced CL intensity and the shift of the transition energy at the outcrop of the threading dislocation. Note that the maps are taken from one and the same dislocation for all temperatures.

The red and the blue lobes in the maps in Figs. 3(e)–3(h) correspond to regions of tensile and compressive strain around the dislocation, respectively, and hence demonstrate that this dislocation is of either a or $a+c$ type. Since the screw component induces only shear strain with a minor effect on the band gap, we cannot distinguish edge and mixed dislocations. The line shift increases with temperature and reaches 2.5 meV at 200 K. At the same time, the statistical error of the fits increases due to the thermal quenching of the emission intensity and the resulting increasing noise in the spectra, thus also leading to a higher noise level in the maps.

Figures 4(a) and 4(b) show simulated maps of the spectrally integrated CL intensity and CL spectral-line positions around an edge threading dislocation, respectively. Evidently, the maps are close to the experimentally recorded maps shown in Fig. 3. In the CL intensity map, the dislocation outcrop is associated with a dark spot with a FWHM of about 200 nm. The intensity distribution

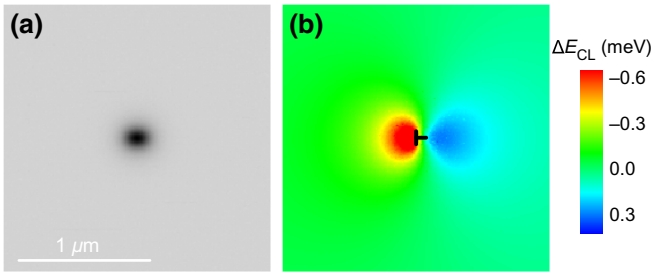

FIG. 4. Monte Carlo calculated maps of (a) the spectrally integrated CL intensity and (b) the CL spectral-line positions for a diffusion length $L = 100$ nm and a temperature of 100 K. The extra half-plane of the dislocation indicates the dislocation position in (b).

Tunneling, Diffusion and nonradiative recombination centers.

$$\frac{\partial n(\mathbf{r};t)}{\partial t} = D_n \Delta n(\mathbf{r};t) + \mathbf{v}\nabla n \quad - \quad n(\mathbf{r};t)\int B(|\mathbf{x}|)p(\mathbf{r}+\mathbf{x};t)d\mathbf{x}$$
$$- \quad n(\mathbf{r};t)\int b_n(|\mathbf{x}|)N_+(\mathbf{r}+\mathbf{x};t)d\mathbf{x}\ .$$

Analogously, the holes are described by the equation

$$\frac{\partial p(\mathbf{r};t)}{\partial t} = D_p \Delta p(\mathbf{r};t) + \mathbf{v}\nabla p - p(\mathbf{r};t)\int B(|\mathbf{x}|)n(\mathbf{r}+\mathbf{x};t)d\mathbf{x}$$
$$- \quad p(\mathbf{r};t)\int b_p(|\mathbf{x}|)[N(\mathbf{r}+\mathbf{x}) - N_+(\mathbf{r}+\mathbf{x};t)]\,d\mathbf{x}\ .$$

Here all the tunneling kernels have the form
$B(|\mathbf{x}|) = B_0 \exp(-|\mathbf{x}|/a)$.

The number of recombination centers waiting for an electron is reduced when the electron is captured, and increased when the hole is captured:

$$\frac{\partial N_+(\mathbf{r};t)}{\partial t} = -n(\mathbf{r};t)\int b_n(|\mathbf{x}|)N_+(\mathbf{r}+\mathbf{x};t)d\mathbf{x} + p(\mathbf{r};t)\int b_p(|\mathbf{x}|)[N(\mathbf{r}+\mathbf{x}) - N_+(\mathbf{r}+\mathbf{x};t)]\,d\mathbf{x}\ .$$

At the initial time $t = 0$, the electrons, holes, and recombination centers are randomly distributed:

$$n(\mathbf{r};0) = \sum_{i=1}^{n_0}\delta(\mathbf{r}-\mathbf{r}_i), \quad p(\mathbf{r};0) = \sum_{j=1}^{n_0}\delta(\mathbf{r}-\mathbf{r}_j), \quad N(\mathbf{r};0) = \sum_{k=1}^{N^{(0)}}\delta(\mathbf{r}-\mathbf{r}_k).$$

At $t = 0$, we can assume that all recombination centers are waiting for an electron, i.e., $N_+(\mathbf{r};0) = N(\mathbf{r};0)$.

The luminescence intensity is given by

$$I(t) = \left\langle \int \frac{1}{|G|} d\mathbf{r} \int B(|\mathbf{x}|) n(\mathbf{r}; t) p(\mathbf{r} + \mathbf{x}; t) d\mathbf{x} \right\rangle$$

where the angle brackets stand for the mathematical expectation with respect to the initial random distribution of electrons, holes and recombination centers, and $|G|$ is the volume of the domain G. The random fields n and p are statistically homogeneous and isotropic, this implies, the correlation function $L_{np}(\mathbf{x}, t) = \langle n(\mathbf{r}, t) p(\mathbf{r} + \mathbf{x}, t) \rangle$ depends only on $|\mathbf{x}|$, the distance between $\mathbf{r}$ and $\mathbf{r} + \mathbf{x}$. We denote by $K_{np}(\mathbf{x}, t)$ the normalized correlation: $K_{np}(\mathbf{x}, t) = L_{np}(\mathbf{x}, t)/n(t)p(t)$. Here $n(t) = \langle n(\mathbf{r}, t) \rangle$ and $p(t) = \langle p(\mathbf{r}, t) \rangle$ since the random fields n and p are homogeneous. In this terms, the intensity reads:

$$I(t) = n(t)p(t) \int B(|\mathbf{x}|) K_{np}(|\mathbf{x}|, t) d\mathbf{x} \ . \qquad (13)$$

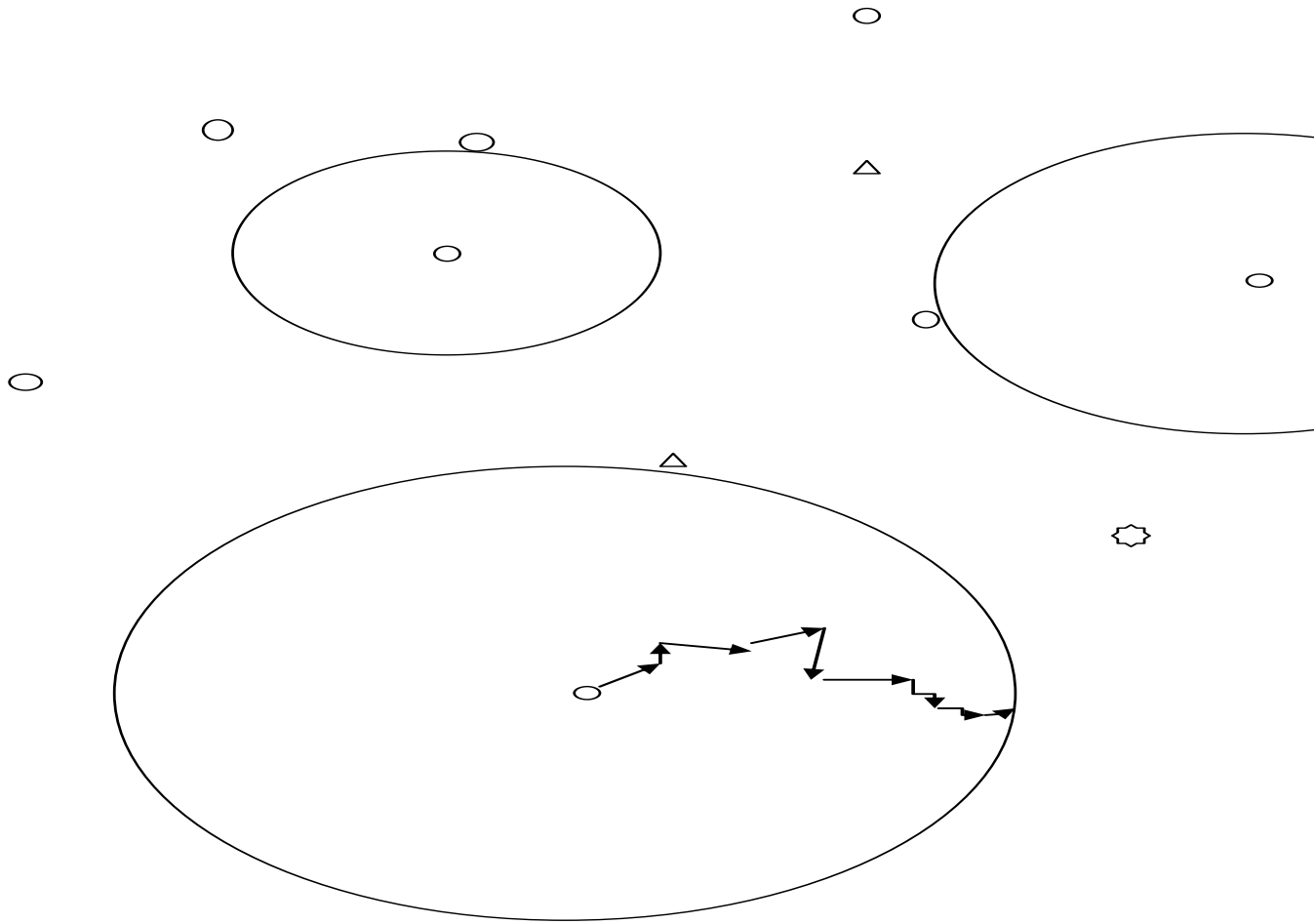

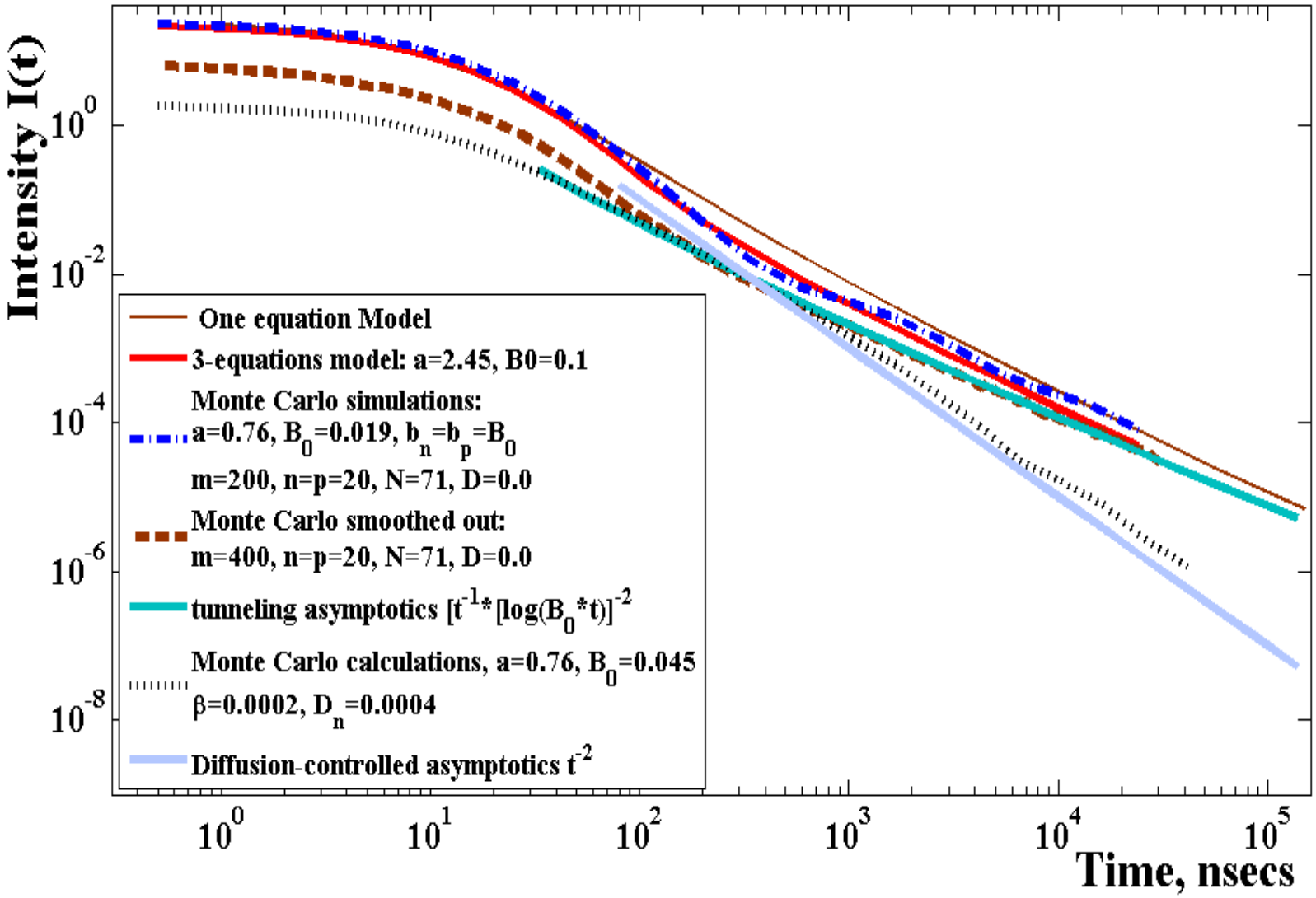
Intensity I(t)
10^{0}
10^{-2}
10^{-4}
10^{-6}
10^{-8}
One equation Model
3-equations model: a=2.45, B0=0.1
Monte Carlo simulations:
a=0.76, B_0=0.019, b_n=b_p=B_0
m=200, n=p=20, N=71, D=0.0
Monte Carlo smoothed out:
m=400, n=p=20, N=71, D=0.0
tunneling asymptotics $[t^{-1}*[\log(B_0*t)]^{-2}$
Monte Carlo calculations, a=0.76, B_0=0.045
β=0.0002, D_n=0.0004
Diffusion-controlled asymptotics t^{-2}
10^{0}
10^{1}
10^{2}
10^{3}
10^{4}
10^{5}
Time, nsecs

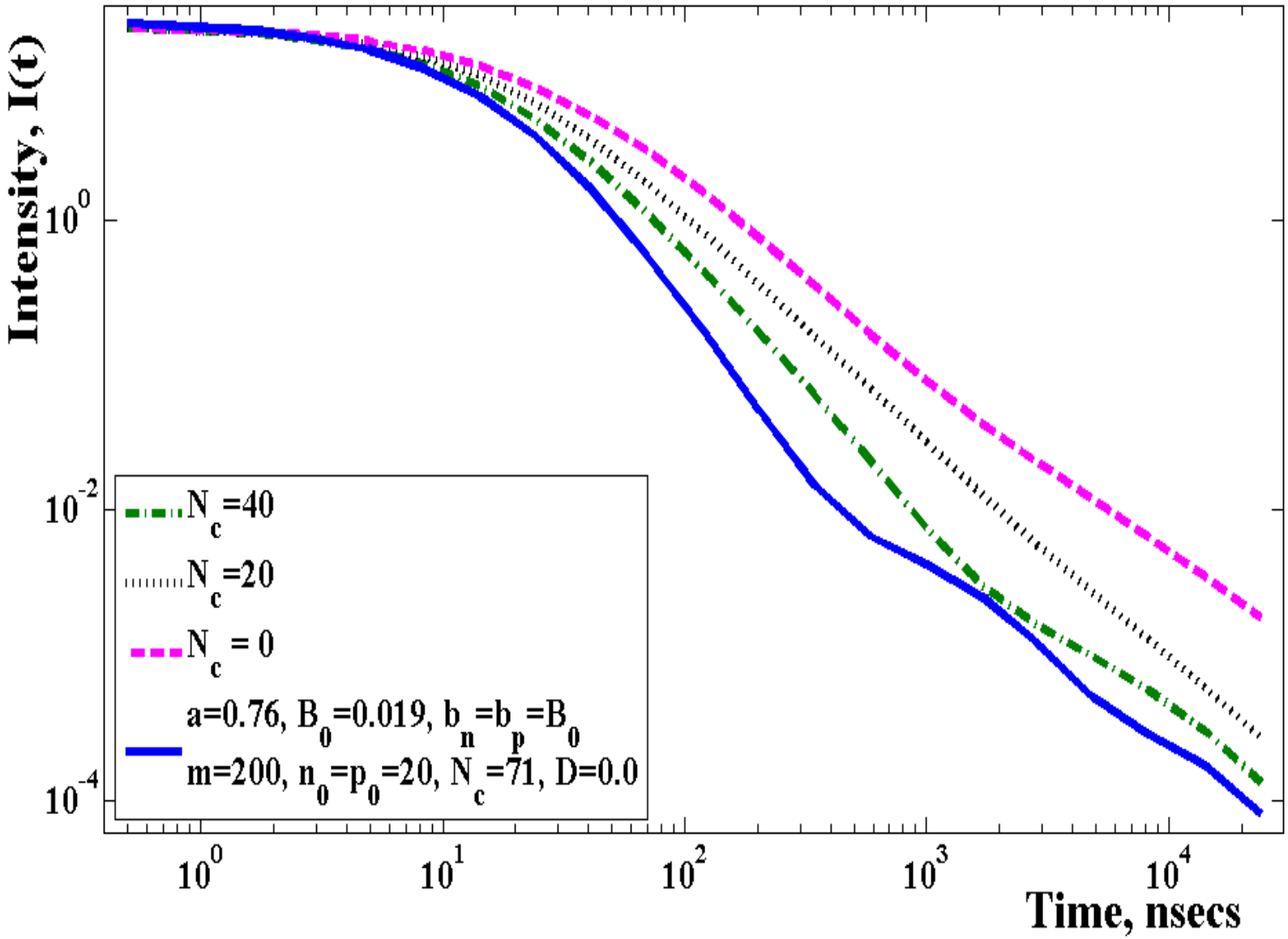
Intensity, I(t)
10^0
10^{-2}
10^{-4}
N_c=40
N_c=20
N_c = 0
a=0.76, B_0=0.019, b_n =b_p =B_0
m=200, n_0 =p_0 =20, N_c =71, D=0.0
10^0
10^1
10^2
10^3
10^4
Time, nsecs

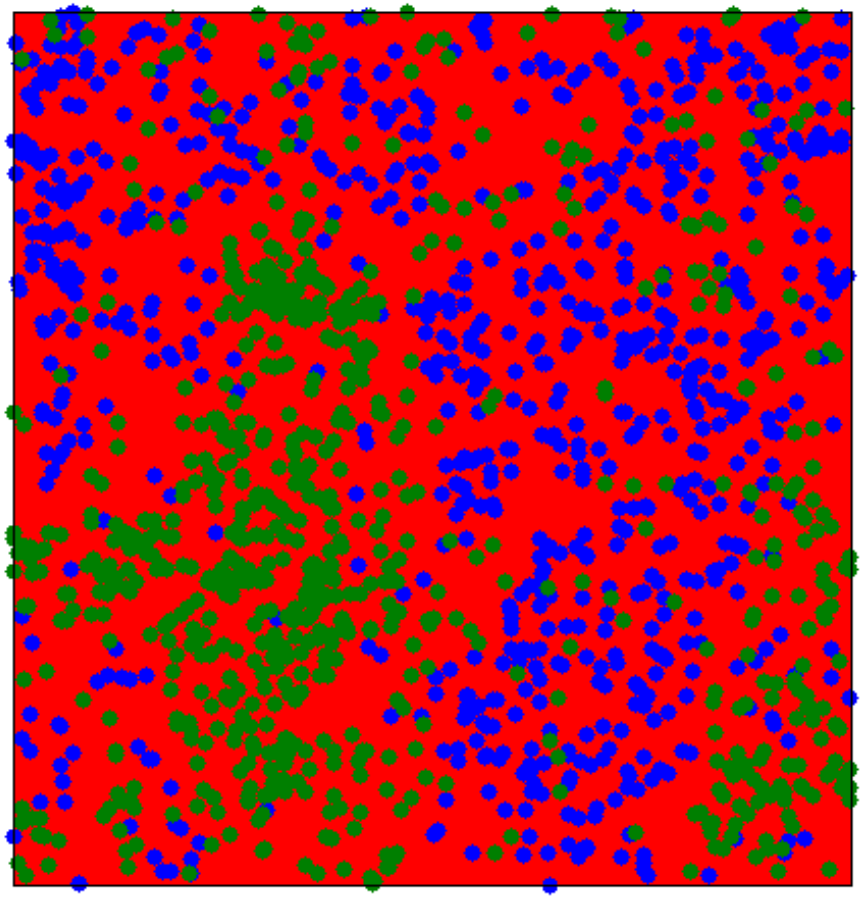

Рис. : Simulation result for the stationary case. Segregation.

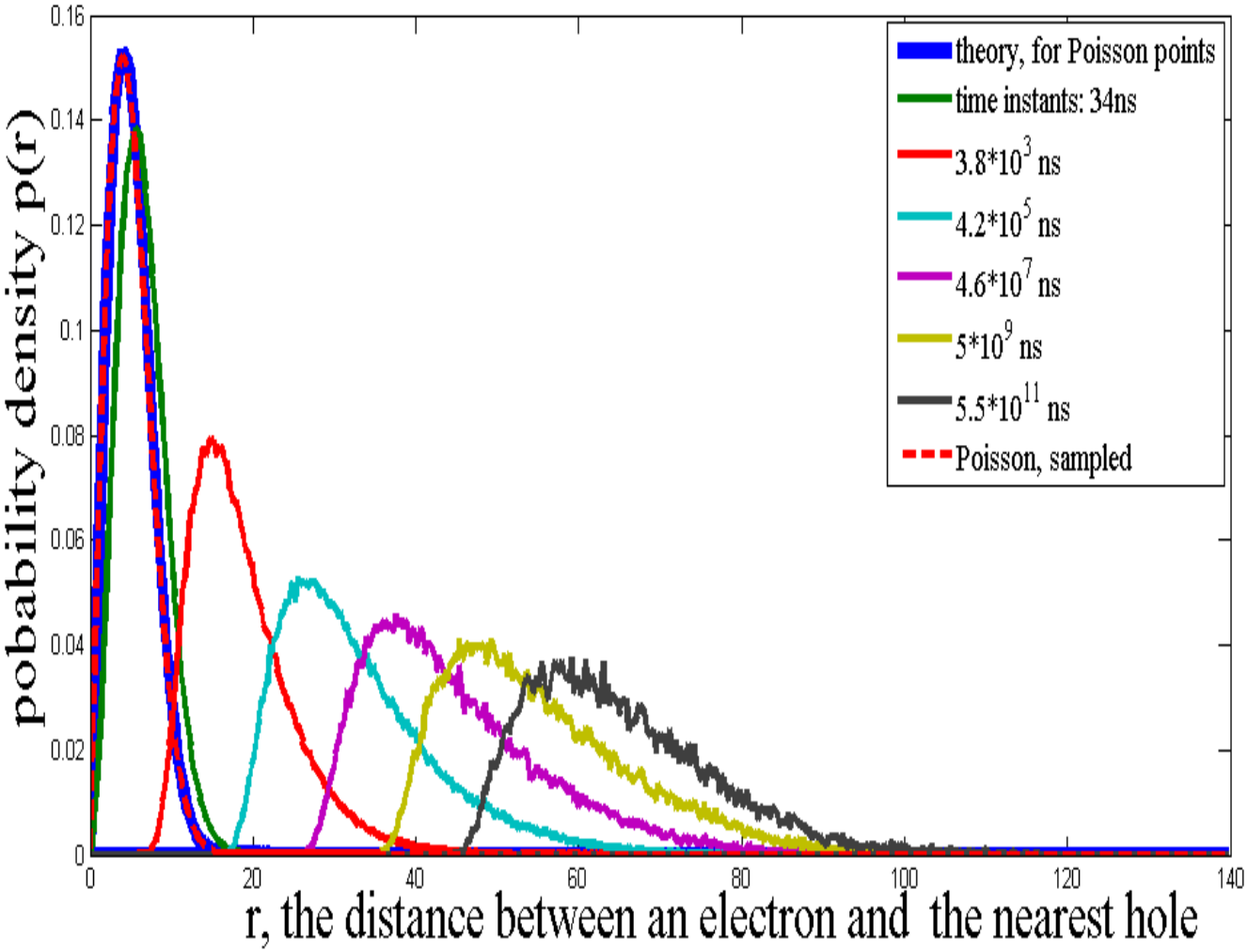

Рис. : Probability density function of the distance from an electron to the nearest hole.

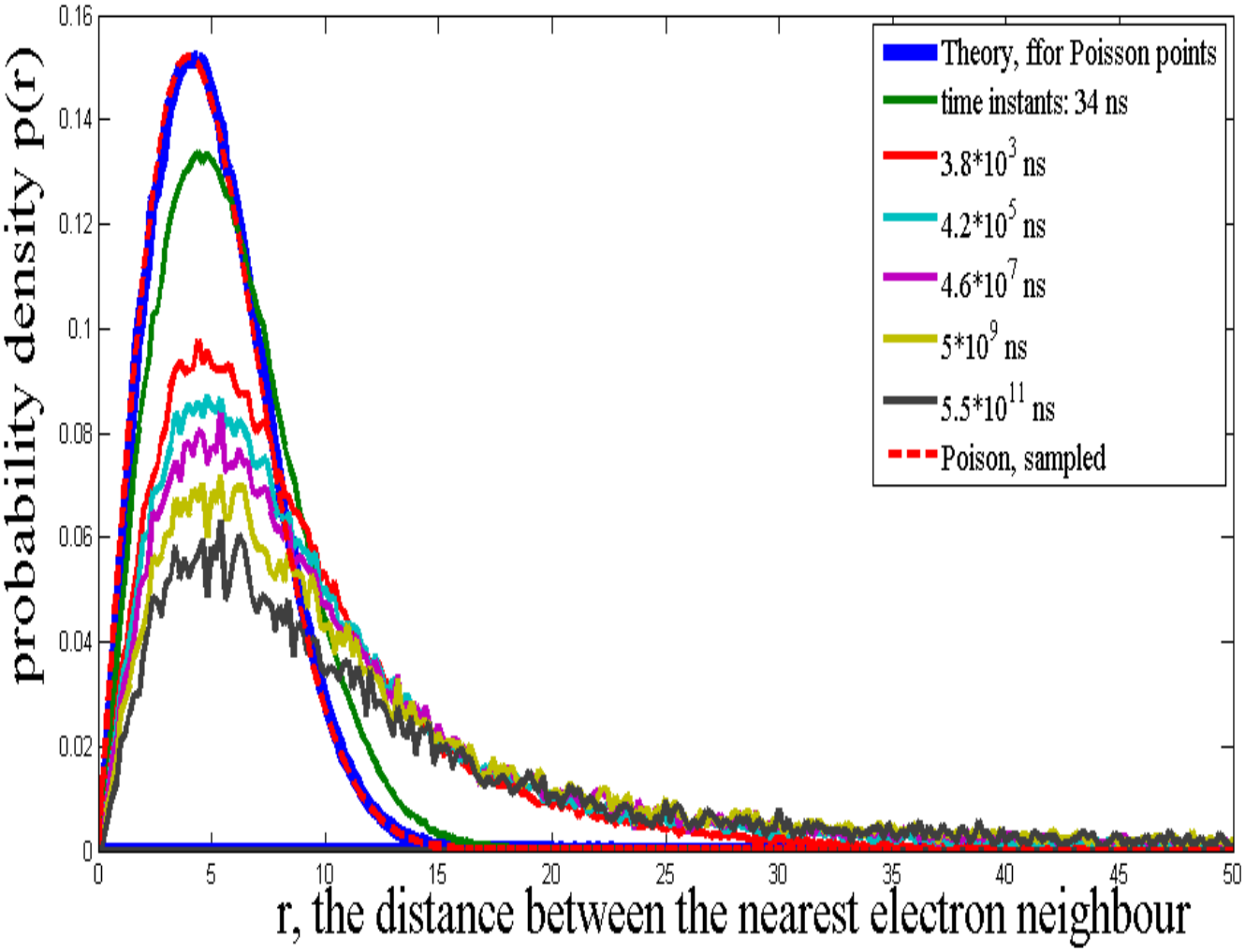

Рис. : Probability density function of the distance from an electron to the nearest electron.

Stochastic Simulation of Fluctuation-Induced Enzyme Kinetics in Vicinity of Traps, Based on Probabilistic Tunneling and Diffusion Mechanisms

K.K. Sabelfeld
Institute of Computational Mathematics and Mathematical Geophysics, Russian Academy of Sciences,
Lavrentiev Prosp. 6, 630090 Novosibirsk, Russia
karl@osmf.sscc.ru

***Abstract*—A stochastic algorithm for simulation of fluctuation-induced enzyme kinetics is developed. The method is generally well applicable when the reactions occur in low-dimensional and disordered media such as biological ones. We suggest a generalization of the Michaelis - Menten scheme of enzyme kinetics that is extended to simulate the quantum tunneling phenomena in the catalytic cycles of enzymatic processes. The stochastic method is suggested as a generalization of the technique developed in our recent studies [12], [13] where this method was developed to describe the annihilation of spatially separate electrons and holes in a disordered semiconductor. The stochastic technique is based on the spatially inhomogeneous, nonlinear integro-differential Smoluchowski equations with random source term. We focus in this study on the spatial distribution, and numerically investigate the segregation in the case of a source with a continuous generation in time and randomly distributed in space. The stochastic particle method presented is based on a probabilistic interpretation of the underlying process as a stochastic Markov process of interacting particle system in discrete but randomly progressed time instances. The segregation is analyzed through the correlation analysis of the vector random field of concentrations which appears to be isotropic in space and stationary in time.**

Keywords: Enzyme kinetics, generalized Michaelis - Menten scheme, tunneling, fluctuation-induced reactions, first passage time, segregation

I. Introduction

Conventional enzyme kinetics equations are derived from the mass-action laws, without taking into account fluctuations, so they may fail in low-dimensional and disordered media such as biological one [1]. Note that many cellular reactions occur in two-dimensional membranes. This is an important aspect to take into account, because in 2D, the impact of fluctuations my be very high, especially in inhomogeneous case. Next important mechanism not taken into account in the mass-action law equations is the tunneling. A fascinating group of enzymes has been shown to possess multiple active sites connected by intramolecular tunnels for the passage of reactive intermediates from the site of production to the site of utilization [19]; see also [4], [9], [3]. In this paper we suggest a generalization of the classical Michaelis - Menten scheme of enzyme kinetics which will include inhomogeneity, the diffusion and tunneling mechanisms, as well as obstacles and traps.

The Michaelis - Menten scheme of enzyme kinetics is a paradigmatic model in biochemistry. It consists in a set of three elementary chemical reactions

$$E + S \underset{k_{-1}}{\overset{k_1}{\rightleftarrows}} C \overset{k_2}{\to} E + P \tag{1}$$

where E,S,P, and C stand for enzyme, substrate, product and enzyme-substrate complex, respectively. The reaction rates are given by k_1, k_{-1}, and k_2.

The mean concentrations are usually described by the kinetics equations

$$\begin{aligned} \frac{d\rho_E}{dt} &= -k_1\rho_E(t)\rho_S(t) + (k_{-1}+k_2)\rho_C(t) \\ \frac{d\rho_C}{dt} &= k_1\rho_E(t)\rho_S(t) - (k_{-1}+k_2)\rho_C(t) \\ \frac{d\rho_S}{dt} &= -k_1\rho_E(t)\rho_S(t) + k_{-1}\rho_C(t) \\ \frac{d\rho_P}{dt} &= k_2\rho_C(t) \end{aligned} \tag{2}$$

with the given initial concentrations at the time $t = 0$.

Such description of chemical reactions implies conditions such that the rate at which the reactants approach each other (the diffusion rate) is much larger than the rate at which they react chemically. Hence, the basic assumption underlying this reaction model is a homogeneous spatial distribution of particles during the reaction at any time instant, i. e., the components E,S,P, and C should be always perfectly mixed.

In this approach, the diffusion is treated macroscopically, ignoring density fluctuations. In the absence of nonlinear interactions such as chemical reactions, the macroscopic diffusion equations govern uniform concentration distributions. Thermal fluctuations, initial density inhomogeneities, and the randomness of reaction events lead to non-uniform concentration fields and changes the solution structure drastically, in particular, the time dependence of the mean solution for asymptotically long times.

The appearance of stable forms or patterns from previously homogeneous spatial conditions is a central issue in biology. The physical mechanisms underlying this symmetry breaking are still largely unknown. Fluctuations are responsible for the spatial correlations, and in particular, they may lead to

segregation, i. e., the formation of spatially separated clusters composed entirely of particles of one type (say, E, or S). In this study we show by computer simulation of the reaction kinetics that the spatial inhomogeneity leads to segregation, and moreover, the segregation holds even in the stationary regime, with characteristic spatial correlations.

Let us explain this by a simple example by considering a reaction of two types of particles, A and B, leading to a product P: $A + B \to P$. The simplest kinetic approach to this reaction first considered by Smoluchowski [17] is based on the rate equations

$$\begin{aligned} dn_A/dt &= -g\, n_A(t) n_B(t), \\ dn_B/dt &= -g\, n_A(t) n_B(t), \\ n_A(0) &= a_0, n_B(0) = b_0 \end{aligned}$$

where g is the reaction rate. For diffusion-controlled reactions in $\mathbf{R}^3$, Smoluchowski obtained $g = 4\pi D r_0$, where r_0 is the particle radius and D is the relative diffusion coefficient. This equation can be easily solved explicitly: $n_A(t) = a_0/(1 + a_0 g t)$ for $a_0 = b_0$, and $n_A(t) = a_0 f_0/[b_0 \exp(f_0 g t) - a_0]$ for $a_0 < b_0$, where $f_0 = b_0 - a_0$.

It was first shown by Ovchinnikov and Zeldovich [10] that in the fluctuation-induced reactions, the long-time asymptotics is $\sim t^{-3/4}$ if $a_0 = b_0$. Generally, for $a_0 = b_0$, the asymptotics $\sim t^{-d/4}$ is valid for any dimensionality $d \leq 4$, while for $d \geq 4$, $\sim t^{-1}$. This law was obtained by several authors using different arguments (see, e. g., Refs. [10], [2], [7], and [12]). If the densities of the components are not equal, the asymptotics is different. For instance, if $a_0 < b_0$, $n_A \sim a_0 \exp(-\sqrt{t})$ for $d = 1$, $n_A \sim a_0 \exp\{-t/\log(t)\}$ for $d = 2$, while for $d \geq 3$, the asymptotic law again coincides with the homogeneous case: $n_A \sim a_0 \exp(-t)$ [2].

II. Generalized Michaelis - Menten model

Now we are ready to generalize the Michaelis - Menten scheme to the spatial inhomogeneous case, where both tunneling and spatial diffusion mechanisms are taken into account:

$$\begin{aligned} \frac{\partial \rho_E}{\partial t} &= D_E \Delta \rho_E(t,\mathbf{r}) - k_1 \rho_E(t,\mathbf{r}) \rho_S(t,\mathbf{r}) \\ &\quad + (k_{-1} + k_2) \rho_C(t,\mathbf{r}) \\ &\quad - \rho_E(t,\mathbf{r}) \int K_1(|x|) \rho_S(t,\mathbf{r}+\mathbf{x})\, d\mathbf{x} \\ \frac{d\rho_C}{dt} &= D_C \Delta \rho_C + k_1 \rho_E(t) \rho_S(t) - (k_{-1} + k_2) \rho_C \\ \frac{d\rho_S}{dt} &= D_S \Delta \rho_S - k_1 \rho_E(t) \rho_S(t) + k_{-1} \rho_C \\ &\quad - \rho_S(t,\mathbf{r}) \int K_1(|x|) \rho_E(t,\mathbf{r}+\mathbf{x})\, d\mathbf{x} \\ \frac{d\rho_P}{dt} &= D_P \Delta \rho_P + k_2 \rho_C(t) \end{aligned} \tag{3}$$

This system of equations is solved in a spatial domain G, with prescribed boundary and initial conditions. The initial conditions: at time $t = 0$ the concentrations are given, for instance, they are all zero in the case we have a source of incoming molecules. Or, when we deal with instantaneous sources of, say, molecules E and S, the concentrations $\rho_E(0,\mathbf{x})$ and $\rho_S(0,\mathbf{x})$ are given functions describing the spatial distributions of E and S in the space. Note that these distributions may be even random, for example, describing the random uniform distribution in G. Periodic boundary conditions are usually used, but any other conditions (absorption, reflection, or partial reflection on the boundary) can be posed.

Let us give some comments to the terms of this equation. When compared to the classical Michaelis - Menten scheme (2), the main difference is in the spatial inhomogeneity, and relevant appearance of the Laplace operators with the diffusion coefficients, and the integral terms as well. The integrals describe the tunneling, meaning, that there is a probability $K_1(|\mathbf{x}|) = k_1 \exp(-|x|/a)$ that the reaction $E+S$ may happen at a random distance $|x|$; here a is a characteristic mean tunneling distance. To simplify the presentation, we have not included the relevant terms which are responsible for the traps and obstacles. Also, the source terms of E and S, if any, are omitted.

The main idea of Monte Carlo methods for solving the spatially homogeneous Smoluchowski equation comes from the probabilistic interpretation of the evolution of the interacting particles as a Markov chain (see, e. g., [6]). In Refs. [11], [14], [5] and [16], [15] we have applied the Monte Carlo technique to homogeneous and inhomogeneous Smoluchowski equations. In this paper, we consider the general inhomogeneous case with diffusion and tunneling. Note that the direct Monte Carlo simulation of the particle interactions and diffusion jumps on a grid is computationally expensive, because one has to consider a huge number of jumps per one particle interaction [1]. In [12], [13] we suggest a new Monte Carlo method for this case, introducing "long diffusion jumps" which accelerate the simulation process significantly.

III. Monte Carlo Algorithms

The structure of the equations (3) is similar to that of the inhomogeneous Smoluchowski coagulation equations, as mentioned in the introduction. The Smoluchowski equations can be interpreted probabilistically as an equation generated by Markov chains describing the evolution of pairwise interacting particle system. In [5]), we developed a Monte Carlo algorithm for inhomogeneous Smoluchowski equation, which we adapt in [12]. Here it will be used to solve the equation (3) for the two-dimensional case $d = 2$, with the focus on the segregation problem.

To initialize the process, a set of molecules S and E are uniformly and independently distributed over a $L \times L$ square G. Then, also uniformly and independently, we place at random the set of obstacles and traps. Since our phase space is continuous, we have to define the reaction event. In the case of the reaction via tunneling, the E and S molecules react on a random distance which is defined bellow. In the case of the reaction due to diffusion, the molecules react (or are trapped by traps) if the two particles are in a sphere of radius ε, ε being sufficiently small, depending on the reaction type. To simplify the notations, we use here the non-normalized number concentrations, so ρ_E and ρ_S stand for the numbers of E and S molecules in the modelling system, respectively.

Assume we have a configuration of E, S, C, P molecules, with a set of obstacles and traps. Now we have to choose

$$p(t,0,1)=\sum_{n=1}^{\infty}\frac{\mu_n}{J_1(\mu_n)}\,\exp\Big\{-\frac{\mu_n^2\,t}{2}\Big\}\,.$$

After the exit time τ_1 is simulated, the exit time from a disc of radius R of a diffusing molecule with diffusion coefficient D is calculated as $\tau=\tau_1 R^2/2D$.

Notice that the random exit time τ_1 can be efficiently simulated by the Walker's method after a discretization of the density $p(t,0,1)$, see for details [12].

IV. Simulation results

As mentioned in the introduction, inhomogeneous fluctuations lead to the formation of clusters. The clustering slows down the reaction considerably, because only particles near the boundary of the clusters are likely to react, while particles inside the cluster have to diffuse to the boundary before they have a chance to react with a particle of the other type. In other words, fluctuations induce the formation of a mosaic of continuously growing domains which contain only one of the reacting components.

The S and P molecule segregation into S-rich and P-rich regions is clearly visible from the four panels of Figure 1. Here we used the reaction probabilities as proportional to $k_1=$, k_{-1} and k_2 and equal to 0.97, 0.02 and 0.04, respectively. The initial concentrations of E and S molecules were taken equal to zero, while the random sources produced these molecules randomly and uniformly distributed over the domain G with the mean intensity 0.01. We show three samples for three different time instances when the system has reached a quasi-stationary state. It should be noted that the simulations are in a good agreement with the theoretical conditions on the clustering phenomenon existence given in [8]. In the case of instantaneous source, the segregation is even more pronounced.

V. Summary and conclusion

A stochastic model which generalizes the classical Michaelis - Menten scheme by extension to inhomogeneous in space systems, where the reactions may be controlled both by diffusion and tunneling is developed. This model is based on a nonlinear system of inhomogeneous 2D integro-differential Smuluchowski equations with random source term. A Monte Carlo simulation algorithm is constructed which solves the relevant 2D Smuluchowski equations for simulation of enzymes kinetics. Both tunneling and diffusion mechanisms are taken into account. Also, traps and obstacles are included in the model. We focus in this study on the spatial distribution, and numerically investigate the segregation in the case of an instantaneous and stationary working source. The method is easily extended to the case of a source with continuous generation in time and randomly distributed in space. The stochastic particle method presented is based on a probabilistic interpretation of the underlying process as a stochastic Markov process of interacting particle system in discrete but randomly progressed time instances.

The author kindly acknowledges the support of the Russian Science Foundation under Grant 14-11-00083.

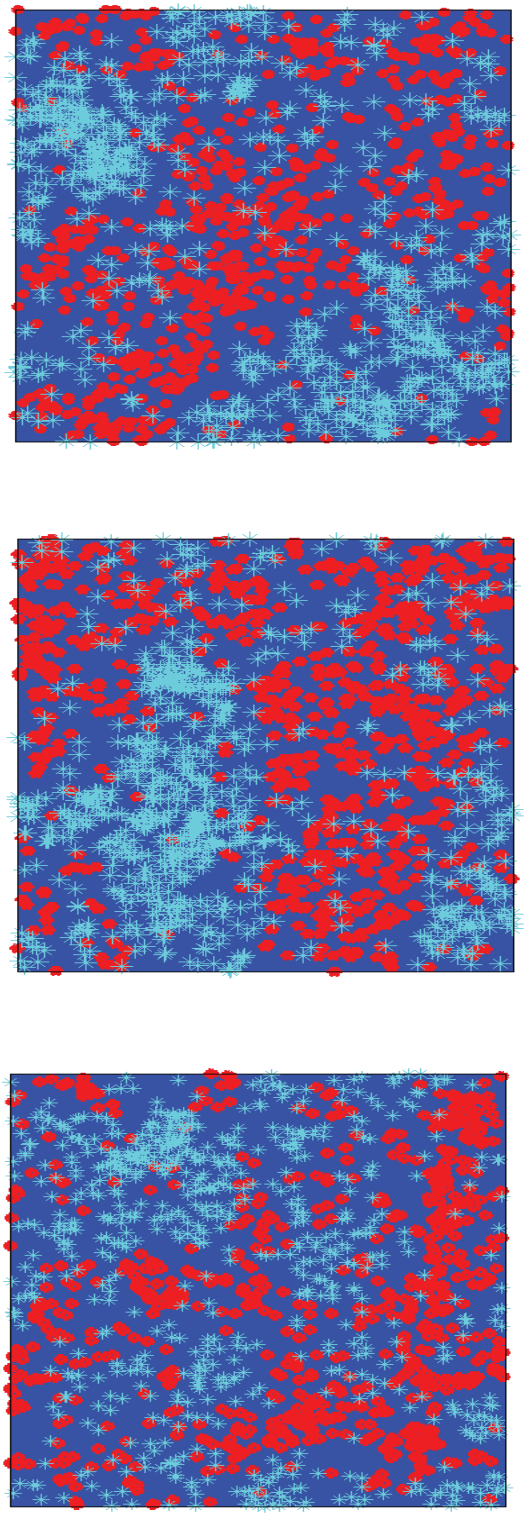

Figure 1. Different samples of S and P molecules during the stochastically stationary regime on a square domain. It is seen, that a segregation is formed with a characteristic distance between large S-rich and P-rich islands.

Синтезирование нановискеров (нанопроводников, нанопроволок) методом пучковой молекулярной эпитаксии открыло новые возможности создания инновационных опто-электронных элементов и инициировало фундаментальные исследования в области формирования наноструктур - нуклеации, коаллесценции и роста кристаллов различной размерности и структуры. Экспериментальные исследования трудоемки, дороги, процесс экспериментов по отслеживанию спонтанного роста занимает много времени. Цель данной технологии - научиться выращивать ансамбли нановискеров заданной структуры. Параметры - распределения по высотам, радиусам, при заданных плотностях и покрытии.

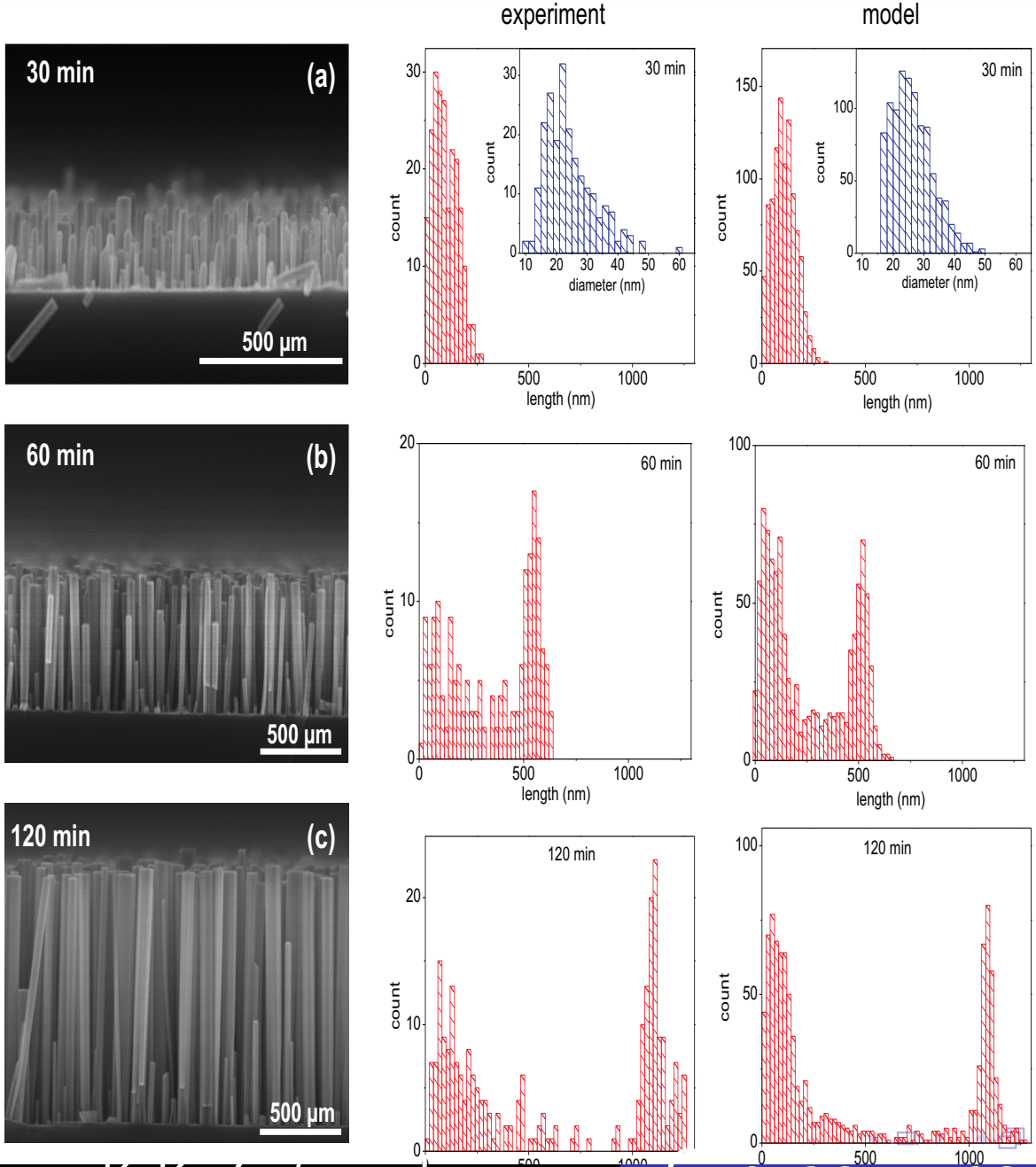
experiment
model
30 min
(a)
500 μm
60 min
(b)
500 μm
120 min
(c)
500 μm
count
length (nm)
diameter (nm)

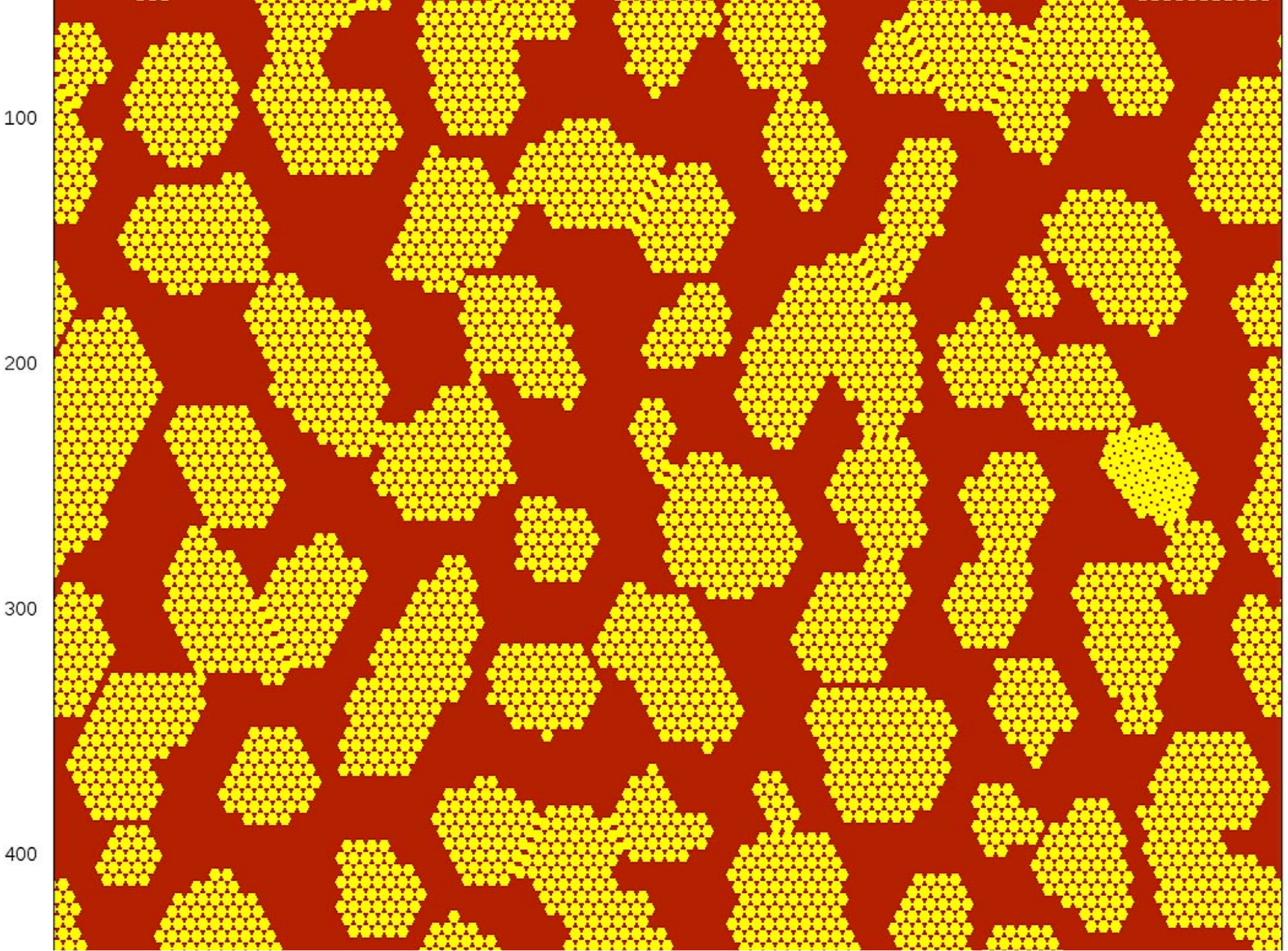
100
200
300
400

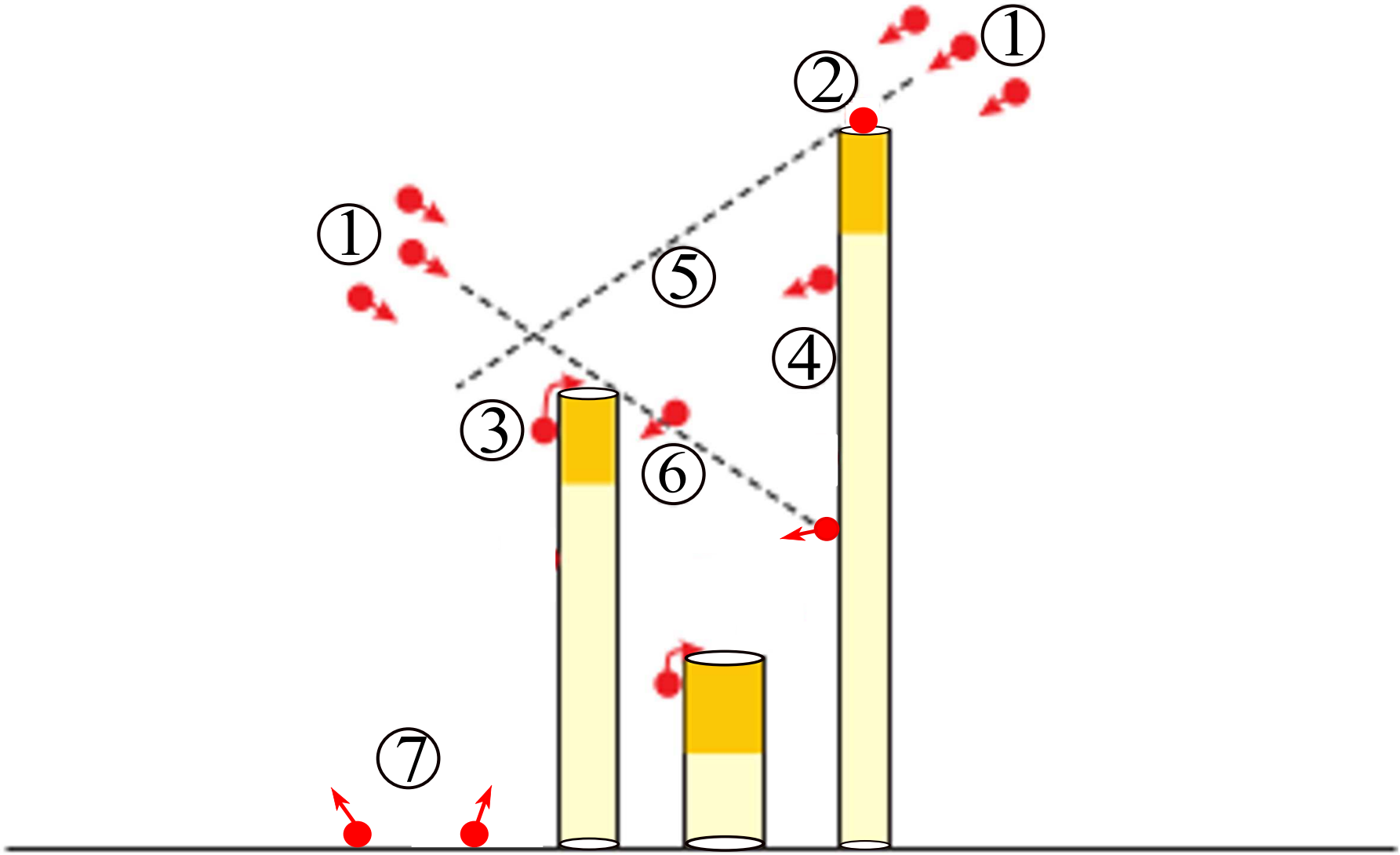

Рис. i

Траектории атомов: в вакууме атомы летят по прямой, попадая на верхнюю поверхность нановискера, поглощаются и дают вклад в его рост. При попадании на боковую поверхность атомы диффундируют с заданным коэффициентом диффузии, могут при этом (1) достичь верхней поверхности, (2) десорбировать, отразиться по Ламберту, и пересечь поверхность одного из окружающих его нановискров, (3) достичь подложки, и также испытать диффузионное отражение.
Процесс дифузии моделируется в соответствии с теоремой взаимности, то есть атом, попадая на поверхность i-го нановискера на высоте $z < h_i$, не отслеживается в своем движении, а переходит на верхнюю поверхность нановискера, или на подложку, либо десорбирует в соответствии с заданными вероятностями.

Вероятность перехода на верхнюю поверхность нановискера с вкладом в его рост

$$p_{up} = \frac{\sinh(\lambda z)}{\sinh(\lambda h_i(t))} , \quad \lambda = 1/L ,$$

вероятность перехода на нижниюю границу нановискера и поглощения (или отражения) на подложке

$$p_{down} = \frac{\sinh(\lambda(h_i(t) - z))}{\sinh(\lambda h_i(t))},$$

и вероятностью десорбции $p_{des} = 1 - p_{up} - p_{down}$.

Случайная высота z, с которой происходит десорбция, моделируется по плотности

$$p(z_0 \to z|\, t) = \frac{\sinh \frac{z_<}{L} \sinh \frac{h(t)-z_>}{L}}{4L \sinh \frac{h(t)}{2L} \sinh \frac{(h(t)-z_0)}{2L} \sinh \frac{z_0}{2L}}\,, \qquad 0 \le z \le h(t)\,, \tag{14}$$

где $z_> = \max(z, z_0)$, $z_< = \min(z, z_0)$.

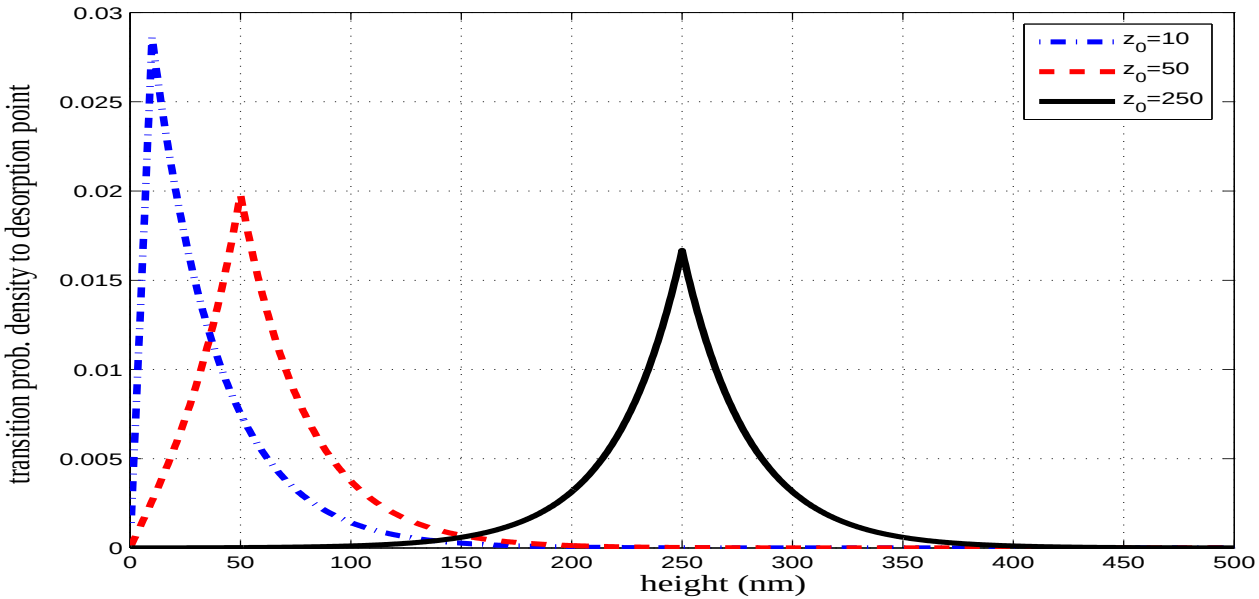

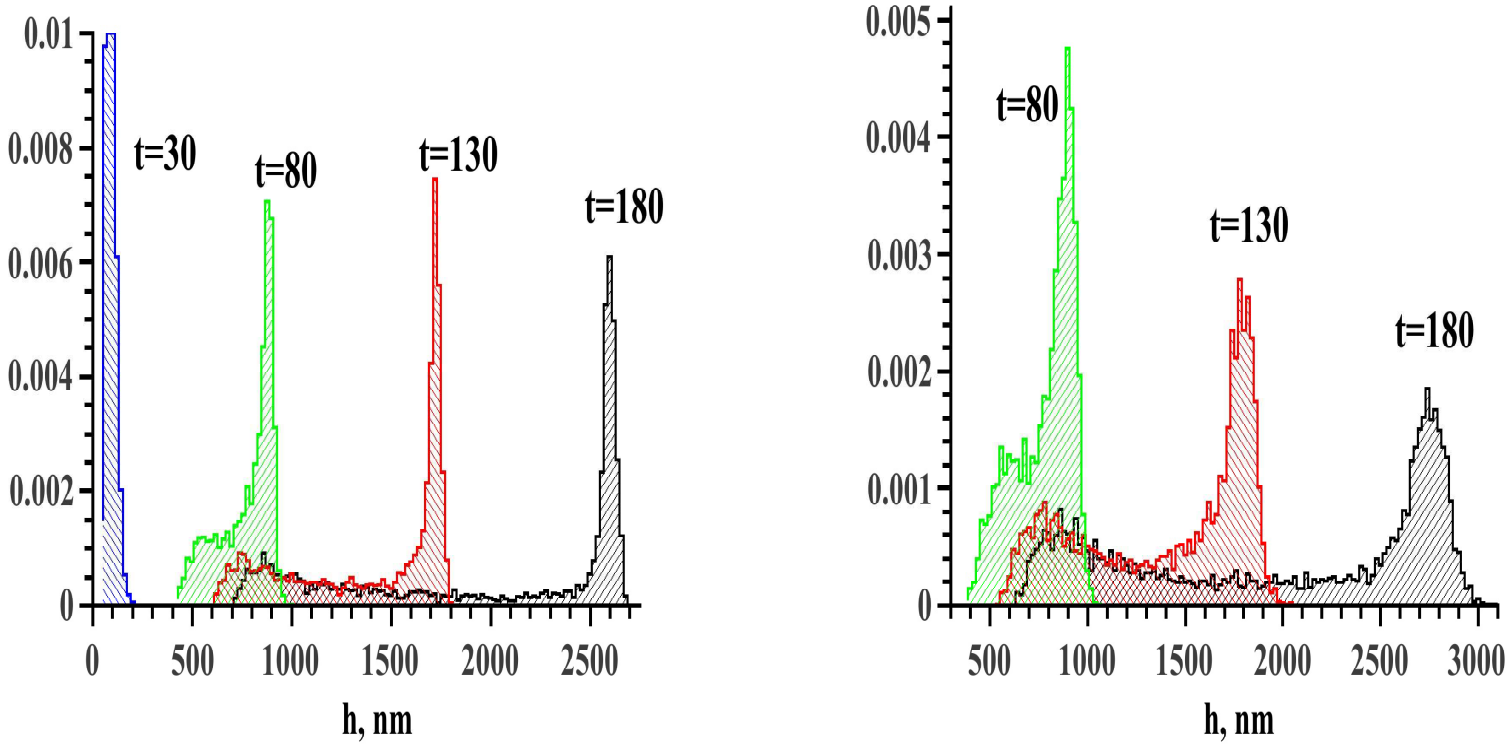

а) б)

Рис. : Эволюция плотности распределения высот нановискеров без учета коаллесценции $L = 50$ а) $\mathbf{V}r = 0.1$ б) $\mathbf{V}r = 2$

компьютеров.

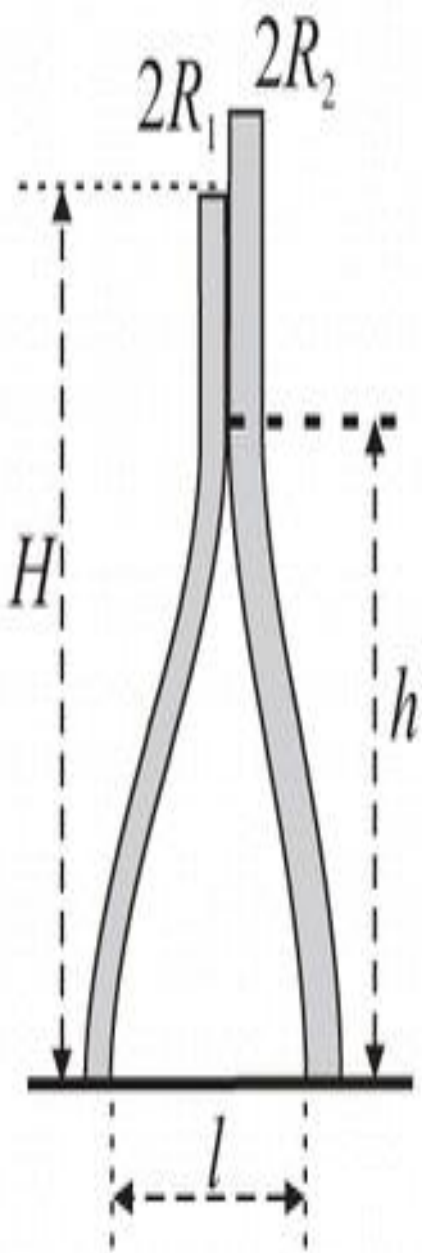

1. Предварительно для каждого нановискера $k = 1, \ldots, N$ и его ближайщего соседа вычисляется наименьшая высота $h_{min}^{(k)}$, при которой возможна их коаллесценция:

$$h_{min}^{(k)} = 4 \left(\frac{l_k^2}{9\gamma R_{min}^{(k)}} \frac{l_1^{(k)} l_2^{(k)}}{l_1^{(k)} + l_2^{(k)}} \right)^{1/4}, \tag{15}$$

где $\gamma = 0.53 * 10^{-2}$ nm,
$l_i^{(k)} = \pi \left(R_i^{(k)} \right)^4 /4, i = 1, 2,\ R_{min}^{(k)} = \min(R_1^{(k)}, R_2^{(k)}),\ l_k$ – расстояние между нановискерами.
2. Для всех $k = 1, \ldots, N$ проверяется выполнения неравенства

$$h_{min}^{(k)} < \min(h_1^{(k)}, h_2^{(k)}). \tag{16}$$

где $h_1^{(k)}$ и $h_2^{(k)}$ – высота k-ого нановискера и его ближайщего соседа.

3. Если выполнено неравенство (16) с некоторой заданной вероятностью $p_{coal}^{(s)}$ моделируется их объединение. Вновь бразовавшийся конгломерат вновь является цилиндром с радиусом $R^{(k)}$ и высотой $h^{(k)}$:

$$R^{(k)} = \sqrt{\left(R_1^{(k)}\right)^2 + \left(R_2^{(k)}\right)^2},\ h^{(k)} = \frac{h_1^{(k)}\left(R_1^{(k)}\right)^2 + h_2^{(k)}\left(R_2^{(k)}\right)^2}{\left(R^{(k)}\right)^2}. \tag{17}$$

Центр нового нановискера $(X^{(k)}, Y^{(k)})$ помещается в общий центр масс объединившихся нанокристаллов с центрами в точках $\left(x_1^{(k)}, y_1^{(k)}\right)$ и $\left(x_2^{(k)}, y_2^{(k)}\right)$:

$$X^{(k)} = x_1^{(k)} + P^{(k)}\left(x_2^{(k)} - x_1^{(k)}\right),\ Y^{(k)} = y_1^{(k)} + P^{(k)}\left(y_2^{(k)} - y_1^{(k)}\right), \tag{18}$$

где

$$P^{(k)} = M_2^{(k)}/(M_1^{(k)} + M_2^{(k)}),\ M_i^{(k)} = h_i^{(k)}\left(R_i^{(k)}\right)^2,\ i = 1, 2$$

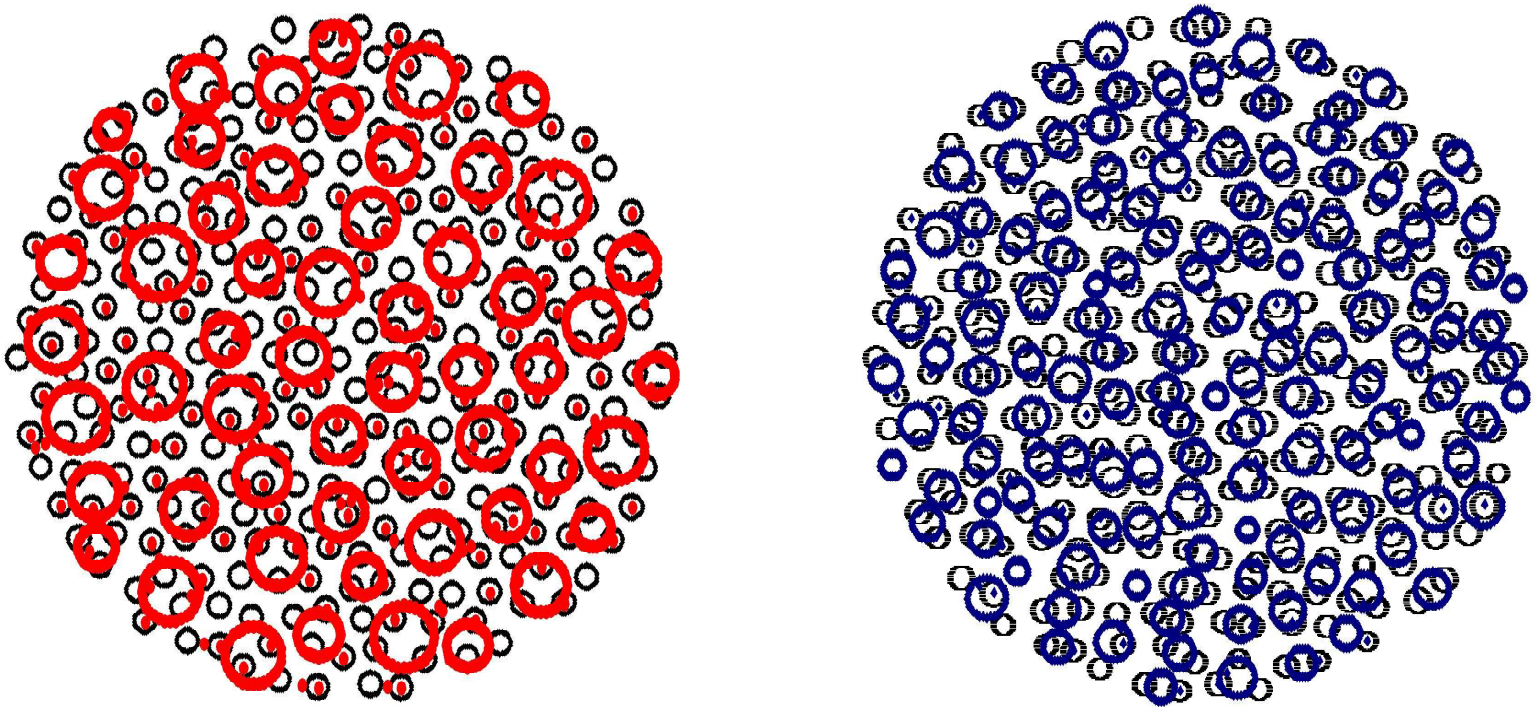

а) б)

Рис. : Реализация случайного расположения нановискеров для $\Delta S = 0.3$, черные мелкие окружности – начальное положение нановискеров, крупные окружности – положение в конечный момент времени моделирования (а) $A = 0.5$ (б) $A = 0.01$

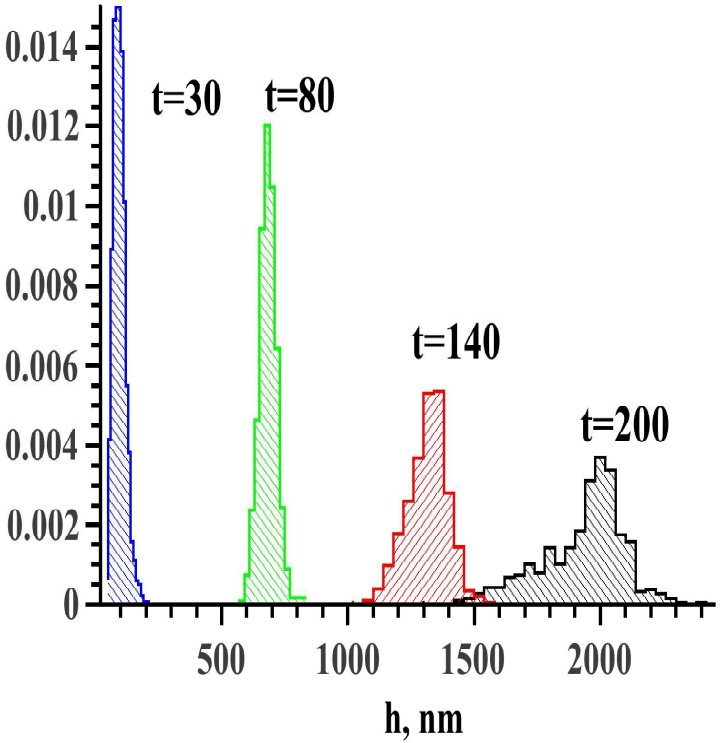

а)

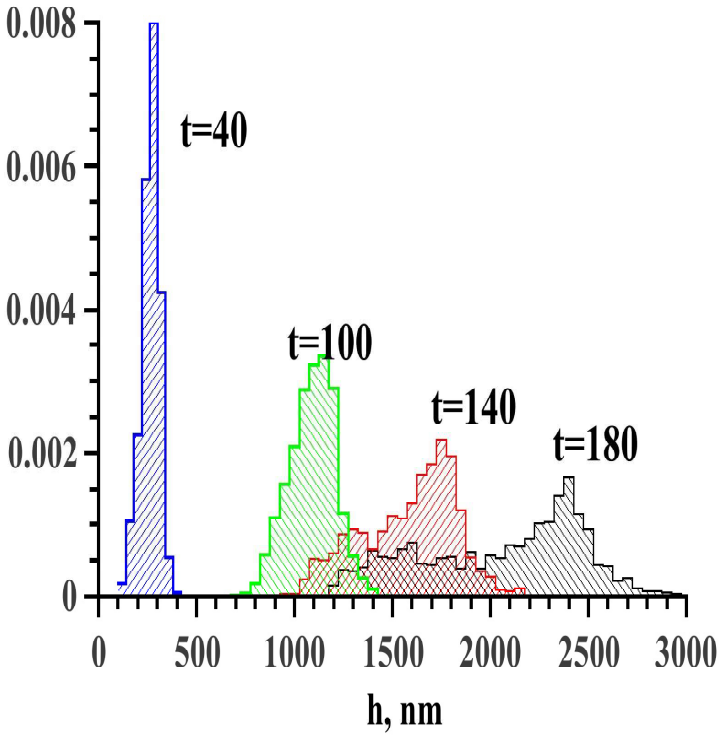

б)

Рис. : Эволюция распределения высот нановискеров с учетом коаллесценции $\Delta S = 0.3$, $\mathbf{E}r = 12$, $\mathbf{V}r = 3$, $A = 0.5$, а) $L = 30$ нм, б) $L = 50$ нм

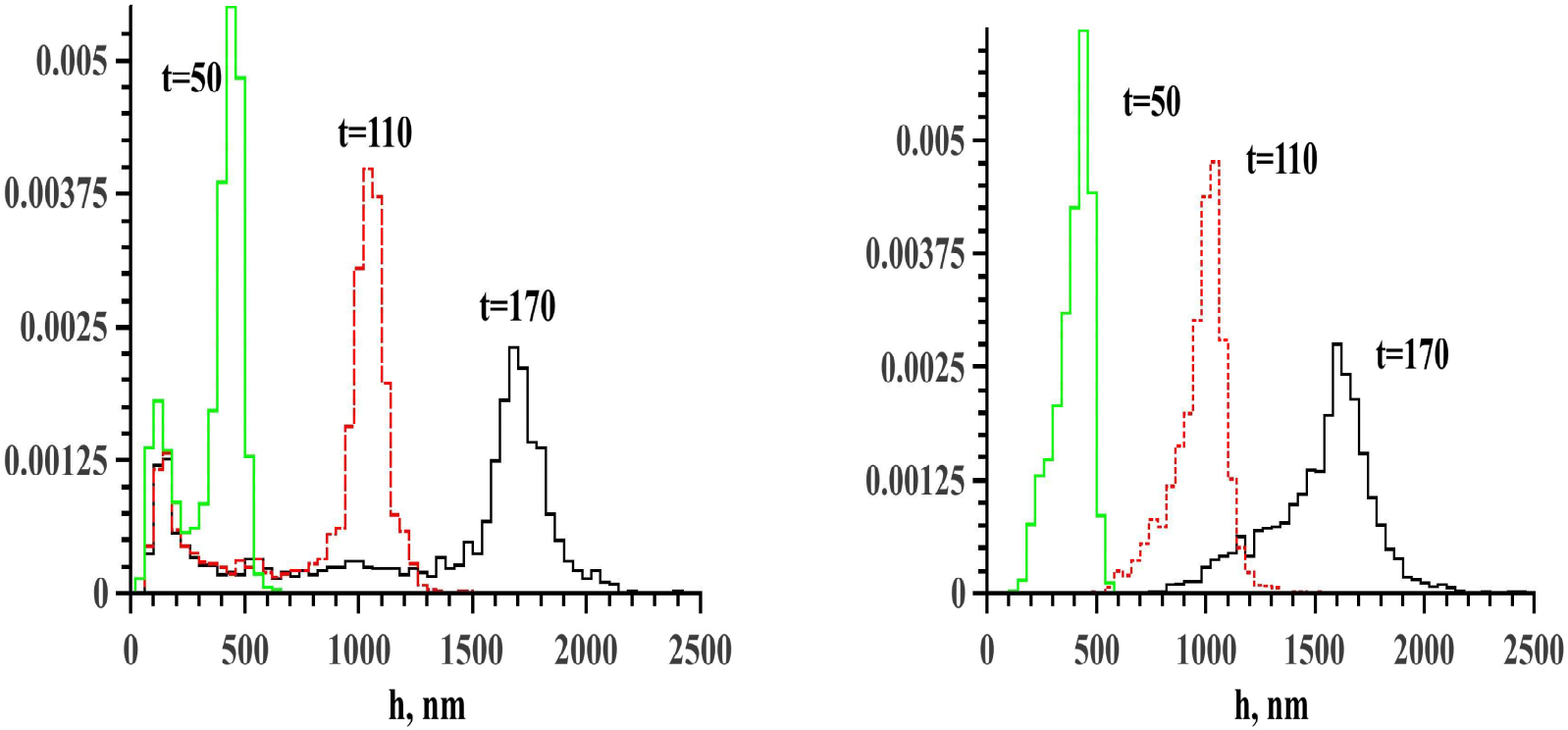

Рис. : Эволюция плотности распределения высот нановискеров при $\Delta S = 0.2$, вероятность адсорбции атомов Ga подложкой $P_{ad} = 0.05$, длина диффузии $L = 30$. слева: учитывается ограничение на адсорбцию атомов Ga боковой поверхностью нановискеров в случае малой вероятности $p(z, t)$, $B = 2$; справа: данное ограничение не учитывается.

Thanks a lot for your attention !